genomic insertions in retroviruses and exogenous gene dilution in adenoviruses.[23] Although electroporation is efficient for introducing exogenous genes into host cells, its cytotoxicity as a result of electrical stimulation cannot be estimated.[24] Transfection reagents, such as PEI and lipofectamine, can form complexes with plasmid DNAs (i.e., polyplexes), causing inefficient delivery of plasmid DNAs into target cells. However, cell viability is largely preserved and this method is safe for clinical use. Therefore, this method is relatively more promising than others for medical applications, provided its efficiency is improved. Many scientists have already reported the use of MNPs in basic research to increase the transfection efficiency of cultivated cells.[8-13,15,16,25] However, the mechanism of MNP gene delivery and gene expression is not yet completely understood; it has still not been optimized for clinical applications, and here, we have discussed the following 3 issues: cellular uptake, endosomal escape, and cytotoxicity.

The uptake of nanoparticles by cells occurs via several mechanisms, which comprise passive transport and active endocytosis; the latter is further classified into nonspecific and receptor-mediated endocytosis.[26] Magnetoplexes and polyplexes are reportedly internalized via caveolae- or clathrin-mediated endocytosis.[25,27-29] The uptake of these complexes is limited by size (up to hundreds of nanometer). The influence of the size of nanoparticles on endocytosis has been investigated using poly(D,L-lactide-co-glycolide) nanoparticles fractionated into small (<100 nm) and large (>100 nm) sizes,[30] gold nanoparticles stratified to 45, 70, and 110 nm,[31] and latex fluorescent beads of defined size (50-1,000 nm).[32] These studies showed that a high rate of cellular internalization could be achieved with smaller-sized nanoparticles. Other research groups, including ours, have previously tested several types of PEI as a coating material for gene transfer, showing that a linear type of 25-kDa PEI was the optimal for γ-Fe_2O_3.[16,33,34] Moreover, we reported that the size limitation for endocytosis using the same nanoparticles with DNA plasmids was <500 nm.[25] Using an *N*-alkyl-PEI2k coating modification on MNPs, the average nanoparticle size was 54.7 ± 9.5 nm, with less cytotoxicity.[35] Cell-penetrating peptides, including low-molecular weight protamines[36] and Tat peptide,[37] have also been demonstrated to be capable of translocating conjugated materials into cells, regardless of their size or hydrophilicity. These surface coatings should effectively support the engulfment of nanoparticles by cells. To enhance the efficiency of gene delivery using MNPs, it is important to control the size of MNPs and their complexes. In this study, we used nonuniformly sized PEI-MNPs (Supplementary Figure 2); therefore, establishment of a method for synthesizing uniformly sized PEI-MNPs should enhance their gene transfection efficiency.

Exogenous materials internalized via endocytosis are engulfed into endosomes, which eventually become lysosomes, where enzymatic decay processes occur.[38] This physiological reaction may be related to the reduced expression of GFP. To circumvent this decay, the release of cargos into the cytosol prior to endosomal escape ameliorates gene expression during gene transfer. Several mechanisms have been proposed to achieve this aim, including pore formation in the endosomal membrane, pH-buffering effect (also known as the proton sponge effect) in the case of PEI,[39] fusion with the endosomal membrane, and photochemical disruption of the endosomal membrane. Some synthetic endosomolytic peptides such as arginine-rich cell penetrating peptides[40] and an analogue of glycoprotein H from herpes simplex virus[41] have been reported to enhance gene expression. The latter approach has been reported to increase the expression levels in human cells by up to 30-fold. Thus, a combination of an endosomal escape agent with this system may potentially reach a clinical stage.[42]

We previously reported that a variety of ferrite nanoparticles, such as Fe_3O_4, $CoFe_2O_4$, $MgFe_2O_4$, and $NiFe_2O_4$, were characterized with regard to their magnetic properties and cytotoxicity in cultured human cells.[43] For striking a balance between magnetization and biocompatibility, Fe_3O_4 could be a suitable agent for gene transfer. In this study, γ-Fe_2O_3 was used, which has properties similar to those of Fe_3O_4. Although PEI modifications can be executed onto each nanoparticle, other nanoparticles may be less balanced. At present, superior coating materials are being developed, such as low molecular weight alkyl-polycation,[35] cationic stearic acid-grafted PEI copolymers and anionic poly(ethylene glycol)-poly(γ-benzyl-L-glutamate),[44] aminodextran, 3-aminopropyltriethoxysilane, and dimercaptosuccinic acid.[45] These reagents can be combined to produce nanoparticles with high magnetization but lower biocompatibility, although they may improve the separation efficacy with negligible cytotoxicity.

The major gene delivery method of episomal vectors is currently electroporation. However, this method does not guarantee a high efficacy of gene transfer, which was only 10%-20% in our experiment. When we attempted to increase the efficacy of gene transfer in electroporation, the cytotoxicity also increased, resulting in cell death. Poor gene transfer efficacy and high cytotoxicity correspond to the size of episomal vectors. Episomal vectors generally contain a promoter sequence, target cDNA sequence, *EBNA-1* sequence of approximately 2,000 bp, *OriP* sequence of approximately 2,200 bp, and drug-resistant genes; these elements contribute to their large size. The size of an episomal vector without target cDNA may exceed 8,000 bp. PEI-MNPs can easily bind to episomal vectors through electrostatic interaction.[46] In a previous study, we demonstrated that the addition of PEI-MNPs could improve plasmid gene transfer.[16] In this study, in comparison with the conventional transfection reagent method, we succeeded in developing a more efficient transfection method using episomal vectors. Although an approximately 2-fold increase in efficacy was achieved, our new strategy resulted in a transfection efficiency of only 2%. However, we established a novel procedure to enrich cells containing PEI-MNPs *in vitro*. To the best of our knowledge, this is the first report to demonstrate that PEI-MNPs themselves could drive PEI-MNP-containing cells and express an exogenous gene under the influence of magnetic field *in vitro*; however, the concept of MNPs themselves driving cells under magnetic field has been previously presented.[47] Further, although the sensitivity of our novel procedure was satisfactory, the specificity remains to be improved, i.e., the separation procedure needs to be improved as the positive population that passed through the magnetic field contained a significant proportion of the negative population. Given the more powerful magnetic properties of

MNPs or stronger magnetic fields through the column or both,[43] could be the purification, not incomplete enrichment. Our protocol could successfully overcome the shortcomings of the large EB virus vector, including poor gene transfer efficacy and high cytotoxicity.

Cell separation by FACS and MACS[48,49] has been widely used in basic and clinical fields. FACS and MACS are used for the separation of heterogeneous cell populations according to their surface antigens or expression of fluorescent proteins in the cell. However, almost all the antibodies used for FACS and MACS are xenogeneic antibodies, which may cause immunological responses in case of cell transplantation. This *in vitro* cell separation was achieved owing to the attraction property of MNPs themselves within the cells under a magnetic field. Our method does not require a cumbersome fluorescent protein inside the cells, fluorescent-conjugated antibody targeting specific cell surface antigens, or additional magnetic materials. We expect that it will become a new strategy for *in vitro* cell separation. Thus, *in vitro* cell separation coupled to gene transfer through the EB virus vector should become a standard procedure for *ex vivo* gene transfer, particularly in case of direct conversion, which is defined as an alteration in cell fate of terminally differentiated cells via intervention of transcriptional networks.[50]

In this study, using *in vitro* and *in vivo* experiments, we demonstrated a novel multifactorial magnetofection achieved by transfection using PEI-MNPs and an *in vitro* cell separation and enrichment using a magnetic field. Magnetofected cells could be clearly detected around the point of transplantation corresponding to the injection site for a week. Our results suggest that MNP separation using PEI-MNPs should lead to new possibilities not only as transfection reagents but also as separating reagents and contrast agents for MRI. Although further improvements are warranted, this will be a novel strategy for *ex vivo* gene transfer for clinical applications.

Appendix A. Supplementary data

Supplementary data to this article can be found online at http://dx.doi.org/10.1016/j.nano.2014.03.018.

References

1. Leszczynski J. Bionanoscience: nano meets bio at the interface. *Nat Nanotechnol* 2010;**5**(9):633-4.
2. Mura S, Couvreur P. Nanotheranostics for personalized medicine. *Adv Drug Deliv Rev* 2012;**64**(13):1394-416.
3. Kim BY, Rutka JT, Chan WC. Nanomedicine. *N Engl J Med* 2010;**363**(25):2434-43.
4. Hrkach J, Von Hoff D, Mukkaram Ali M, Andrianova E, Auer J, Campbell T, et al. Preclinical development and clinical translation of a PSMA-targeted docetaxel nanoparticle with a differentiated pharmacological profile. *Sci Transl Med* 2012;**4**(128):128ra39.
5. Davis ME, Zuckerman JE, Choi CH, Seligson D, Tolcher A, Alabi CA, et al. Evidence of RNAi in humans from systemically administered siRNA via targeted nanoparticles. *Nature* 2010;**464**(7291):1067-70.
6. Govindarajan S, Kitaura K, Takafuji M, Ihara H, Varadarajan KS, Patel AB, et al. Gene delivery into human cancer cells by cationic lipid-mediated magnetofection. *Int J Pharm* 2013;**446**(1–2):87-99.
7. Li XX, Li KA, Qin JB, Ye KC, Yang XR, Li WM, et al. In vivo MRI tracking of iron oxide nanoparticle-labeled human mesenchymal stem cells in limb ischemia. *Int J Nanomedicine* 2013;**8**:1063-73.
8. Scherer F, Anton M, Schillinger U, Henke J, Bergemann C, Kruger A, et al. Magnetofection: enhancing and targeting gene delivery by magnetic force in vitro and in vivo. *Gene Ther* 2002;**9**(2):102-9.
9. Mykhaylyk O, Antequera YS, Vlaskou D, Plank C. Generation of magnetic nonviral gene transfer agents and magnetofection in vitro. *Nat Protoc* 2007;**2**(10):2391-411.
10. Hughes C, Galea-Lauri J, Farzaneh F, Darling D. Streptavidin paramagnetic particles provide a choice of three affinity-based capture and magnetic concentration strategies for retroviral vectors. *Mol Ther* 2001;**3**(4):623-30.
11. Pandori M, Hobson D, Sano T. Adenovirus-microbead conjugates possess enhanced infectivity: a new strategy for localized gene delivery. *Virology* 2002;**299**(2):204-12.
12. Mah C, Fraites Jr TJ, Zolotukhin I, Song S, Flotte TR, Dobson J, et al. Improved method of recombinant AAV2 delivery for systemic targeted gene therapy. *Mol Ther* 2002;**6**(1):106-12.
13. Huth S, Lausier J, Gersting SW, Rudolph C, Plank C, Welsch U, et al. Insights into the mechanism of magnetofection using PEI-based magnetofectins for gene transfer. *J Gene Med* 2004;**6**(8):923-36.
14. Nel A, Xia T, Madler L, Li N. Toxic potential of materials at the nanolevel. *Science* 2006;**311**(5761):622-7.
15. Kami D, Takeda S, Itakura Y, Gojo S, Watanabe M, Toyoda M. Application of magnetic nanoparticles to gene delivery. *Int J Mol Sci* 2011;**12**(6):3705-22.
16. Kami D, Takeda S, Makino H, Toyoda M, Itakura Y, Gojo S, et al. Efficient transfection method using deacylated polyethylenimine-coated magnetic nanoparticles. *J Artif Organs* 2011;**14**(3):215-22.
17. Zhang H, Xia T, Meng H, Xue M, George S, Ji Z, et al. Differential expression of syndecan-1 mediates cationic nanoparticle toxicity in undifferentiated versus differentiated normal human bronchial epithelial cells. *ACS Nano* 2011;**5**(4):2756-69.
18. Arbab AS, Liu W, Frank JA. Cellular magnetic resonance imaging: current status and future prospects. *Expert Rev Med Devices* 2006;**3**(4):427-39.
19. Kishida T, Asada H, Kubo K, Sato YT, Shin-Ya M, Imanishi J, et al. Pleiotrophic functions of Epstein-Barr virus nuclear antigen-1 (EBNA-1) and oriP differentially contribute to the efficiency of transfection/expression of exogenous gene in mammalian cells. *J Biotechnol* 2008;**133**(2):201-7.
20. Okita K, Hong H, Takahashi K, Yamanaka S. Generation of mouse-induced pluripotent stem cells with plasmid vectors. *Nat Protoc* 2010;**5**(3):418-28.
21. Seki T, Yuasa S, Fukuda K. Derivation of induced pluripotent stem cells from human peripheral circulating T cells. *Curr Protoc Stem Cell Biol* 2011 [Volume 18, Chapter 4:Unit 4 A3.1-4A3.9.].
22. Warren L, Manos PD, Ahfeldt T, Loh YH, Li H, Lau F, et al. Highly efficient reprogramming to pluripotency and directed differentiation of human cells with synthetic modified mRNA. *Cell Stem Cell* 2010;**7**(5):618-30.
23. Huang S, Kamihira M. Development of hybrid viral vectors for gene therapy. *Biotechnol Adv* 2013;**31**(2):208-23.
24. Su CH, Wu YJ, Wang HH, Yeh HI. Nonviral gene therapy targeting cardiovascular system. *Am J Physiol Heart Circ Physiol* 2012;**303**(6):H629-38.
25. Ota S, Takahashi Y, Tomitaka A, Yamada T, Kami D, Watanabe M, et al. Transfection efficiency influenced by aggregation of DNA/polyethylenimine max/magnetic nanoparticle complexes. *J Nanoparticle Res* 2013;**15**:1653-64.
26. Gao Z, Zhang L, Hu J, Sun Y. Mesenchymal stem cells: a potential targeted-delivery vehicle for anti-cancer drug, loaded nanoparticles. *Nanomedicine* 2013;**9**(2):174-84.
27. Lim J, Clements MA, Dobson J. Delivery of short interfering ribonucleic acid-complexed magnetic nanoparticles in an oscillating field occurs via caveolae-mediated endocytosis. *PLoS ONE* 2012;**7**(12):e51350.

28. Rejman J, Bragonzi A, Conese M. Role of clathrin- and caveolae-mediated endocytosis in gene transfer mediated by lipo- and polyplexes. *Mol Ther* 2005;**12**(3):468-74.
29. Tran N, Webster TJ. Understanding magnetic nanoparticle osteoblast receptor-mediated endocytosis using experiments and modeling. *Nanotechnology* 2013;**24**(18):185102.
30. Prabha S, Zhou WZ, Panyam J, Labhasetwar V. Size-dependency of nanoparticle-mediated gene transfection: studies with fractionated nanoparticles. *Int J Pharm* 2002;**244**(1–2):105-15.
31. Wang SH, Lee CW, Chiou A, Wei PK. Size-dependent endocytosis of gold nanoparticles studied by three-dimensional mapping of plasmonic scattering images. *J Nanobiotechnol* 2010;**8**:33.
32. Rejman J, Oberle V, Zuhorn IS, Hoekstra D. Size-dependent internalization of particles via the pathways of clathrin- and caveolae-mediated endocytosis. *Biochem J* 2004;**377**(Pt 1):159-69.
33. Wiseman J, Goddard C, McLelland D, Colledge W. A comparison of linear and branched polyethylenimine (PEI) with DCChol/DOPE liposomes for gene delivery to epithelial cells in vitro and in vivo. *Gene Ther* 2003;**10**(19):1654-62.
34. Thomas M, Lu JJ, Ge Q, Zhang C, Chen J, Klibanov AM. Full deacylation of polyethylenimine dramatically boosts its gene delivery efficiency and specificity to mouse lung. *Proc Natl Acad Sci U S A* 2005;**102**(16):5679-84.
35. Liu G, Wang Z, Lu J, Xia C, Gao F, Gong Q, et al. Low molecular weight alkyl-polycation wrapped magnetite nanoparticle clusters as MRI probes for stem cell labeling and in vivo imaging. *Biomaterials* 2011;**32**(2):528-37.
36. Suh JS, Lee JY, Choi YS, Yu F, Yang V, Lee SJ, et al. Efficient labeling of mesenchymal stem cells using cell permeable magnetic nanoparticles. *Biochem Biophys Res Commun* 2009;**379**(3):669-75.
37. Coupland PG, Fisher KA, Jones DR, Aylott JW. Internalisation of polymeric nanosensors in mesenchymal stem cells: analysis by flow cytometry and confocal microscopy. *J Control Release* 2008;**130**(2):115-20.
38. Varkouhi AK, Scholte M, Storm G, Haisma HJ. Endosomal escape pathways for delivery of biologicals. *J Control Release* 2011;**151**(3):220-8.
39. Boussif O, Lezoualc'h F, Zanta MA, Mergny MD, Scherman D, Demeneix B, et al. A versatile vector for gene and oligonucleotide transfer into cells in culture and in vivo: polyethylenimine. *Proc Natl Acad Sci* 1995;**92**(16):7297-301.
40. Kay MA, Glorioso JC, Naldini L. Viral vectors for gene therapy: the art of turning infectious agents into vehicles of therapeutics. *Nat Med* 2001;**7**(1):33-40.
41. Tu Y, Kim JS. A fusogenic segment of glycoprotein H from herpes simplex virus enhances transfection efficiency of cationic liposomes. *J Gene Med* 2008;**10**(6):646-54.
42. Lehner R, Wang X, Marsch S, Hunziker P. Intelligent nanomaterials for medicine: carrier platforms and targeting strategies in the context of clinical application. *Nanomedicine* 2013;**9**(6):742-57.
43. Tomitaka A, Jeun M-H, Bae S-T, Takemura Y. Evaluation of magnetic and thermal properties of ferrite nanoparticles for biomedical applications. *J Magn* 2011;**16**(2):164-8.
44. Guo RM, Cao N, Zhang F, Wang YR, Wen XH, Shen J, et al. Controllable labelling of stem cells with a novel superparamagnetic iron oxide-loaded cationic nanovesicle for MR imaging. *Eur Radiol* 2012;**22**(11):2328-37.
45. Calero M, Gutiérrrez L, Salas G, Luengo Y, Lázaro A, Acedo P, et al. Efficient and safe internalization of magnetic iron oxide nanoparticles: two fundamental requirements for biomedical applications. *Nanomedicine* 2013, pii: S1549-9634(13)00675-8.
46. Namgung R, Singha K, Yu MK, Jon S, Kim YS, Ahn Y, et al. Hybrid superparamagnetic iron oxide nanoparticle-branched polyethylenimine magnetoplexes for gene transfection of vascular endothelial cells. *Biomaterials* 2010;**31**(14):4204-13.
47. Majewski AP, Schallon A, Jerome V, Freitag R, Muller AH, Schmalz H. Dual-responsive magnetic core-shell nanoparticles for nonviral gene delivery and cell separation. *Biomacromolecules* 2012;**13**(3):857-66.
48. Fulwyler MJ. Electronic separation of biological cells by volume. *Science* 1965;**150**(3698):910-1.
49. Abts H, Emmerich M, Miltenyi S, Radbruch A, Tesch H. CD20 positive human B lymphocytes separated with the magnetic cell sorter (MACS) can be induced to proliferation and antibody secretion in vitro. *J Immunol Methods* 1989;**125**(1–2):19-28.
50. Ieda M, Fu JD, Delgado-Olguin P, Vedantham V, Hayashi Y, Bruneau BG, et al. Direct reprogramming of fibroblasts into functional cardiomyocytes by defined factors. *Cell* 2010;**142**(3):375-86.

Seminal vesicle protein SVS2 is required for sperm survival in the uterus

Natsuko Kawano[a], Naoya Araki[b], Kaoru Yoshida[c], Taku Hibino[d], Naoko Ohnami[a], Maako Makino[a], Seiya Kanai[a], Hidetoshi Hasuwa[e], Manabu Yoshida[b,1], Kenji Miyado[a,1], and Akihiro Umezawa[a]

[a]Department of Reproductive Biology, National Center for Child Health and Development, 2-10-1 Okura, Setagaya, Tokyo 157-8535, Japan; [b]Misaki Marine Biological Station, Graduate School of Science, University of Tokyo, Miura, Kanagawa 238-0225, Japan; [c]Biomedical Engineering Center, Toin University of Yokohama, Yokohama 225-8502, Japan; [d]Faculty of Education, Saitama University, 255 Shimo-Okubo, Sakura-ku, Saitama City, Saitama 338-8570, Japan; and [e]Research Institute for Microbial Diseases, Osaka University, Yamadaoka 3-1, Suita, Osaka 565-0871, Japan

Edited by John J. Eppig, The Jackson Laboratory, Bar Harbor, ME, and approved February 11, 2014 (received for review November 12, 2013)

In mammals, sperm migrate through the female reproductive tract to reach the egg; however, our understanding of this journey is highly limited. To shed light on this process, we focused on defining the functions of seminal vesicle secretion 2 (SVS2). *SVS2*$^{-/-}$ male mice produced sperm but were severely subfertile, and formation of a copulatory plug to cover the female genital opening did not occur. Surprisingly, even when artificial insemination was performed with silicon as a substitute for the plug, sperm fertility in the absence of SVS2 remained severely reduced because the sperm were already dead in the uterus. Thus, our results provide evidence that the uterus induces sperm cell death and that SVS2 protects sperm from uterine attack.

in vivo fertilization | uterine sperm selection | decapacitation | acrosomal reaction | uterine spermicide

Fluids secreted from male accessory sex organs are believed to regulate fertility efficiency through the control of sperm functions such as motility and fertilizing ability in vivo (1, 2). Notably, the induced ability of fertilization-competent (i.e., capacitated) rabbit sperm is reverted to an incompetent state when it is mixed with seminal plasma; this phenomenon, discovered by Chang and Bedford (2, 3), is referred to as "decapacitation." Subsequent to their findings, many studies have focused on identifying the decapacitation factor in the seminal plasma using in vitro assays (4–6); the seminal plasma is believed to stabilize sperm plasma membranes and prevent uterine sperm from undergoing premature capacitation and acrosomal reaction, an exocytotic process that occurs immediately before sperm–egg fusion (7, 8).

In mammals the seminal vesicle is an accessory organ within the male reproductive tract, and its secretion influences sperm fertility and embryo development via oviductal expression of cytokines (9). Seminal vesicle secretion 2 (SVS2), a major component of the seminal vesicle secretions, inhibits sperm fertility in vitro, and homologous genes are conserved among many species (10, 11). As described previously (10), SVS2 binds to sperm in the uterus but not to sperm in the oviduct. In addition, SVS2 binds to ganglioside GM1 as its receptor on the sperm membrane, resulting in the control of sperm fertility (11). To study the role of SVS2 in vivo, we here focused on defining a role for SVS2 in in vivo fertilization.

Results

To explore the physiological role of SVS2, we produced mice lacking the *SVS2* gene (*SI Appendix*, Fig. S1). Two independent ES cell lines carrying a mutated allele were used to generate chimeric mice capable of transmitting the mutated allele to their progeny. Homozygous (*SVS2*$^{-/-}$) mice were identified by Southern blot and PCR analyses of genomic DNA. The same results were obtained for both mouse lines used. Breeding yielded the predicted number of null mice at Mendelian frequency. Both male and female *SVS2*$^{-/-}$ mice were born healthy, grew normally, and had normally configured seminal vesicles (Fig. 1*A* and *SI Appendix*, Fig. S2*A*). The loss of SVS2 in the *SVS2*$^{-/-}$ mice was confirmed by SDS/PAGE using total proteins collected from seminal vesicles (Fig. 1*B* and *SI Appendix*, Fig. S3*B*). Moreover, electron microscopic analysis of the seminal vesicle epithelium revealed the presence of normal features, such as secretory organelles, in *SVS2*$^{-/-}$ mice as well as in *SVS2*$^{+/+}$ mice (*SI Appendix*, Fig. S2*B*).

Despite the absence of detrimental effects on seminal vesicle formation, *SVS2*$^{-/-}$ male mice displayed strongly reduced fertility: the average litter size produced by the *SVS2*$^{-/-}$ male mice was significantly smaller (0.63 ± 0.13) than those of the *SVS2*$^{+/+}$ and *SVS2*$^{+/-}$ male mice (5.23 ± 0.53 and 4.96 ± 0.42, respectively; $P < 0.001$) (Fig. 1*C*). Copulatory plugs were not found in female mice mated with *SVS2*$^{-/-}$ male mice (Fig. 1*A*), although mating behavior was observed and sperm were normally produced in these mice (*SI Appendix*, Fig. S4*A*). In addition, the rates of motile and hyperactivated sperm, evaluated by computer assisted sperm analysis (CASA), were indistinguishable between *SVS2*$^{-/-}$ and *SVS2*$^{+/+}$ male mice (*SI Appendix*, Fig. S4 *B* and *C*). When the epididymal sperm of *SVS2*$^{-/-}$ male mice were subjected to in vitro fertilization (IVF), the rate of fertilized eggs (based on the evaluation of pronuclear formation) was comparable to those of sperm from *SVS2*$^{+/+}$ and *SVS2*$^{+/-}$ male mice (*SI Appendix*, Fig. S4*D*). From these results, we concluded that SVS2 might be essential for plug formation but not spermatogenesis or in vitro sperm fertility.

Significance

Male mice lacking seminal vesicle secretion 2 (SVS2) protein, which is a major component of seminal vesicle secretions, display prominently reduced fertility. However, their epididymal sperm are able to fertilize eggs normally in vitro, suggesting that SVS2 is only essential for in vivo fertilization. We demonstrate that infertility in *SVS2*$^{-/-}$ male mice is caused not only by failed copulatory plug formation but also by the disruption of ejaculated sperm in the uterus by uterus-derived cytotoxic factors. SVS2 acts to protect sperm against these uterus-derived cytotoxic factors by coating the sperm surface and preventing uterine attack. Thus, our results provide evidence that mammalian males have developed a protective strategy against female attack at the gamete level.

Author contributions: N.K., K.Y., M.Y., and K.M. designed research; N.K., N.A., T.H., N.O., M.M., S.K., H.H., and K.M. performed research; N.K., M.Y., K.M., and A.U. analyzed data; and N.K. and K.M. wrote the paper.

The authors declare no conflict of interest.

This article is a PNAS Direct Submission.

Freely available online through the PNAS open access option.

[1]To whom correspondence may be addressed. E-mail: yoshida@mmbs.s.u-tokyo.ac.jp or miyado-k@ncchd.go.jp.

This article contains supporting information online at www.pnas.org/lookup/suppl/doi:10.1073/pnas.1320715111/-/DCSupplemental.

DEVELOPMENTAL BIOLOGY

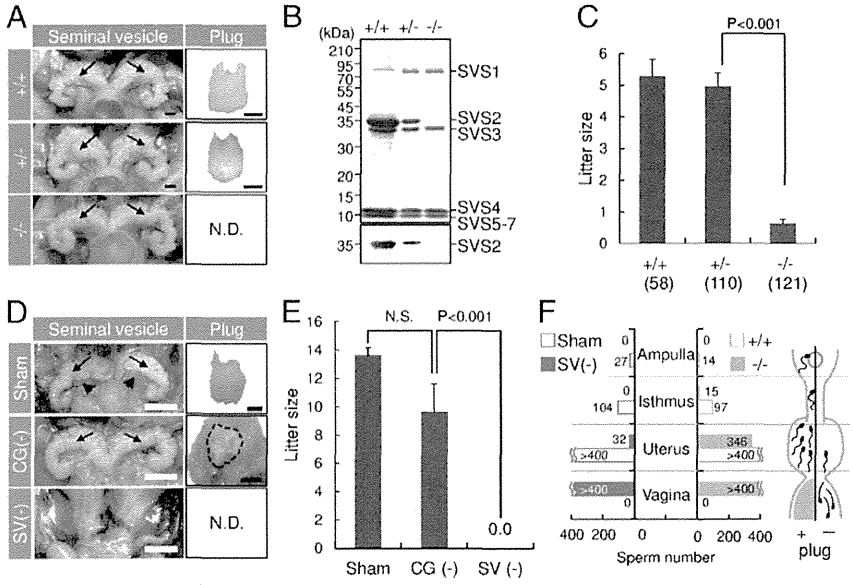

Fig. 1. Impaired copulatory plug formation in *SVS2*$^{-/-}$ and seminal vesicle-excised mice. (*A*) Appearance of seminal vesicles and copulatory plugs. Arrows, seminal vesicles. N.D., not detected. (Scale bars, 2 mm.) (*B*) Immunoblotting of the total inner fluid of seminal vesicles isolated from male mice with anti-SVS2 pAb. (*Upper*) Staining with CBB; (*Lower*) reaction with anti-SVS2 pAb. (*C*) Fecundity of male mice. Parentheses, numbers of male mice examined. (*D*) Appearance of seminal vesicles and copulatory plugs in surgically operated mice. Sham, sham-operated mice; CG(-), mice with coagulating glands excised; SV(-), mice with seminal vesicles excised. Arrows, seminal vesicles; arrowheads, coagulating glands; dotted circle, a representative plug formed by a CG(-) male mouse. (Scale bars, 2 mm.) (*E*) Fecundity of surgically operated male mice ($n = 5$). N.S., not significant. (*F*) Numbers of sperm entering the female reproductive tract after copulation. The total sperm number is indicated as the sum of five independent experiments. (*Right graph*) Number of sperm detected in each sectioned tract of female mice mated with *SVS2*$^{+/+}$ or *SVS2*$^{-/-}$ male mice. (*Left graph*) Number of sperm detected in each sectioned tract of female mice mated with Sham or SV(-) male mice.

The phenotypes of gene-deficient mice are not always related to the disrupted gene itself but are sometimes caused by the disruption of a neighboring gene (12). To examine whether the phenotype observed for *SVS2*$^{-/-}$ mice was directly derived from the lack of SVS2, two transgenic mouse lines expressing SVS2 in the seminal vesicles were generated and introduced into the *SVS2*$^{-/-}$ background. We found that introduction of the transgene recovered plug formation (*SI Appendix*, Fig. S5*A*) and the reduced fecundity in *SVS2*$^{-/-}$ male mice (*SI Appendix*, Fig. S5*B*). These results suggest that SVS2 plays a role in plug formation and imply that loss of plug formation may lead to male infertility.

When the male accessory sex glands, coagulating glands (arrowheads in Fig. 1*D*) or seminal vesicles (arrows in Fig. 1*D*), were surgically removed, the average litter size produced by the mice after coagulating gland removal was 9.6 ± 2.0, which was comparable to that of the control mice (13.6 ± 0.5) (Fig. 1*E*). In contrast, mice that had undergone seminal vesicle removal were still found to be sterile (0.0 ± 0.0; $P < 0.001$) (Fig. 1*E*); Moreover, copulatory plugs were not formed in female mice that were mated with male mice with seminal vesicles removed (Fig. 1*D*, *Bottom*), even though mating behavior, testosterone production, and spermatogenesis in these mice is normal (*SI Appendix*, Fig. S6). Both *SVS2*$^{-/-}$ mice and male mice that had undergone seminal vesicle removal showed failure of copulatory plug formation and leakage of the ejaculated sperm from the uterus, as evidenced by the presence of sperm in the vagina and decreased numbers of sperm in the uterus (Fig. 1*F*). The sperm number in the female reproductive tract was remarkably reduced because of a loss of plug formation. On the other hand, as described recently (13), loss of a copulatory plug strongly reduces the number of uterine sperm and lowers fertility but does not lead to severe subfertility or infertility. Therefore, it was unclear whether the infertility of *SVS2*$^{-/-}$ mice was due to the lack of sperm reaching the egg or other mechanisms.

To address this question, we developed a method for artificial insemination (AI) (Fig. 2*A* and *SI Appendix*, Fig. S7). Briefly, epididymal sperm (5×10^6 sperm/mL) with or without seminal vesicle secretions were injected directly into the uterus of female mice, followed by silicon, which filled the cervix and the vagina as a substitute for a copulatory plug, preventing the sperm from leaving the uterus. To assess sperm fertility in vivo, two-cell embryos developed in the oviduct were counted 25 h after sperm injection. Surprisingly, the direct injection of epididymal sperm into the uterus resulted in a significantly lower rate of two-cell embryo formation in the oviduct (20.4% ± 7.4%) compared with mice that had been injected with epididymal sperm and seminal vesicle secretions (76.0% ± 17.7%; $P = 0.019$) (Fig. 2*B*). To evaluate the effect of SVS2 as a decapacitation factor, we counted the number of acrosome-reacted sperm in the uterus 2 h after sperm injection. The rate of acrosomal reaction was dramatically increased when sperm were injected into the uterus without seminal vesicle secretions [82.7% ± 3.5% using FITC-labeled peanut agglutinin (PNA-FITC); 88.9% ± 1.4% using anti-IZUMO1 mAb; $P < 0.001$], compared with sperm injected with seminal vesicle secretions (PNA-FITC, 9.2% ± 3.1%; anti-IZUMO1, 12.9% ± 2.4%) or during normal copulation (PNA-FITC, 10.3% ± 2.8%; anti-IZUMO1, 14.1% ± 2.3%) (Fig. 2*C* and *SI Appendix*, Fig. S8*A*). These results suggest that the absence of seminal vesicle secretions strongly affects in vivo fertilization.

To assess the in vivo fertility of sperm ejaculated from *SVS2*$^{-/-}$ male mice, we introduced transgenes expressing GFP in the acrosome and RFP in the mitochondria [*B6D2F1-Tg (CAG/su9-DsRed2, Acr3-EGFP) RBGS002Osb*] (14) into the *SVS2*$^{-/-}$ background (*SVS2*$^{-/-}$*Tg*^{RBGS}) (*SI Appendix*, Fig. S8*B*). We then estimated the acrosome reaction rate for sperm ejaculated into female mice. We first confirmed that the disappearance of GFP fluorescence from sperm heads was consistent with the occurrence of an acrosome reaction detected by PNA-FITC and anti-IZUMO1 mAb, 3 h after sperm entered the uterus via copulation

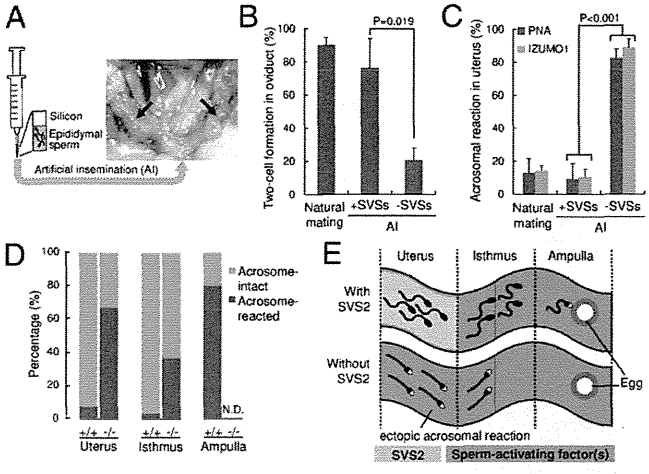

Fig. 2. Sperm fertility with or without SVS2 by AI using silicon as a substitute for the copulatory plug. (*A*) Experimental design of the AI procedure. Arrows, sperm solution coinjected with a blue dye in the uterine cavity. (*B*) Formation of two-cell embryos in oviducts by injection of sperm with or without SVSs using AI. Concomitantly, when female mice were mated with male mice, the number of two-cell embryos formed in oviducts was counted ($n = 6$). (*C*) Rates of acrosome-reacted sperm in the uterus by injection of sperm with or without SVSs using AI. Concomitantly, when female mice were mated with male mice, the number of acrosome-reacted sperm in the uterus was counted ($n = 3$). (*D*) Rates of acrosome-reacted sperm ejaculated from $SVS2^{-/-}$ mice or control mice ($SVS2^{+/+}$and $SVS2^{+/-}$) to the female reproductive tract ($n = 3$). In three parts of the reproductive tract, the number of acrosome-reacted sperm (RFP-positive and GFP-negative) was counted and compared with that of acrosome-intact sperm (RFP-positive and GFP-positive). (*E*) Schematic model of ectopic sperm activation in the absence of SVS2. Sperm with black heads, acrosome-intact sperm; sperm with white heads, acrosome-reacted sperm. Green substance, predicted sperm-activating factor(s).

(*SI Appendix*, Fig. S8*C*). When $SVS2^{-/-}Tg^{RBGS}$ male mice were mated with female mice, the ejaculated sperm were found to enter the uterus without plug formation, although the number of sperm inside the female reproductive tract was reduced compared with control $SVS2^{+/+}Tg^{RBGS}$ and $SVS2^{+/-}Tg^{RBGS}$ mice (*SI Appendix*, Figs. S9 and S10). Furthermore, in these two control mice nearly all sperm had intact acrosomes in the uterus and isthmus of the oviduct 3 h after sperm ejaculation (Fig. 2*D*). In the ampulla of oviduct, an acrosome reaction occurred in more than 80% of ejaculated sperm from the control mice (PNA-FITC, 83.3% ± 16.7%; anti-IZUMO1, 87.5% ± 12.5%) (Fig. 2*D*). In contrast, ejaculated sperm from $SVS2^{-/-}Tg^{RBGS}$ male mice had already undergone the acrosomal reaction inside the uterus (67.0% ± 2.4%) (Fig. 2*D*). In addition, ejaculated sperm from $SVS2^{-/-}Tg^{RBGS}$ male mice were rarely observed in the isthmus of the oviduct but were unable to move into the ampulla (Fig. 2*D*). Because the sperm of $SVS2^{-/-}Tg^{RBGS}$ male mice normally express two factors involved in sperm migration, namely ADAM3 and Catsper2 (*SI Appendix*, Fig. S11 *A* and *B*), we considered that the impaired migration to the oviduct was due to the absence of SVS2. We supposed that in the absence of SVS2 the ejaculated sperm would undergo an acrosomal reaction ectopically inside the uterus as a result of the sperm-activating factor(s) stored there, effectively blocking the entry of sperm into the oviduct (Fig. 2*E*).

To test this hypothesis, we next examined the sperm membrane collected from the uterus via electron microscopic analysis. The three groups examined were the epididymal sperm injected by AI with seminal vesicle secretions (+SVSs), with SVS2 (+SVS2), and without SVS2 (−SVS2). In the case of +SVSs or +SVS2, the sperm membrane remained intact in the uterus and became coated with the seminal vesicle secretions and SVS2 (Fig. 3 *A* and *B*). When the sperm were used for AI without SVS2, the cell and nuclear membranes were fractured not only in the acrosome but in all regions of the sperm (Fig. 3 *A* and *B*). To further examine the membrane disruption of the sperm in the uterus, the sperm were stained with propidium iodide (PI) and eosin (15). Consistent with the electron microscopic analysis, the rate of membrane-disrupted sperm was significantly higher without SVS2 (PI, 72.9% ± 3.4%, $P < 0.001$; eosin, 93.9% ± 2.3%, $P < 0.001$) than with SVS2 (PI, 12.8% ± 3.1%; eosin, 14.0% ± 4.7%) (Fig. 3*C*). From these results we concluded that intrauterine sperm died in the absence of SVS2.

To further examine this concept, we carried out immunohistochemical analysis of intrauterine sperm with or without SVS2 using anti-IZUMO1 mAb (Fig. 3 *D* and *E*). During sperm–egg fusion, IZUMO1 is translocated from the acrosomal membrane to the sperm plasma membrane at the time of acrosomal exocytosis (16), and its distribution is subsequently divided into two types, entire-head type (H-type) and equatorial segment type (17). We categorized the IZUMO1 distribution in the intrauterine sperm without SVS2 into an uncharacteristic type, namely the acrosomal-cap type (AC-type) (Fig. 3*D*). The rate of AC-type distribution was significantly higher in the sperm without SVS2 (83.7% ± 3.1%) than in the sperm mated naturally and the sperm with SVS2 (2.6% ± 0.8% and 0.9% ± 0.6%, respectively; $P < 0.001$) (Fig. 3*E*), indicating that the AC-type sperm were dead. To confirm the cytotoxic effect of uterine fluid (UF), sperm collected from the epididymides of $SVS2^{+/+}$ and $SVS2^{-/-}$ mice were incubated with UF. Consequently, sperm motility decreased in a time-dependent manner and was comparable between $SVS2^{+/+}$ and $SVS2^{-/-}$ mice (*SI Appendix*, Fig. S12 *A* and *B*); the rate of PI-positive dead sperm was similarly increased in both strains (*SI Appendix*, Fig. S12 *C* and *D*). On the other hand, the cytotoxic effect was absent in fluid collected from the ampulla of oviduct (*SI Appendix*, Fig. S13). In the sperm collected from $SVS2^{-/-}$ mice, CD46, whose deficiency in sperm accelerates spontaneous acrosomal reactions (18), was normally expressed and localized in the sperm head (*SI Appendix*, Fig. S11 *C* and *D*). Thus, our results suggest that intrauterine sperm die as a result of direct exposure to UF in the absence of SVS2.

Discussion

We previously reported that SVS2 acts as a decapacitation factor in IVF (10). As expected, the sperm ejaculated from $SVS2^{-/-}$ mice seemed to show ectopic activation in the uterine cavity, resulting in failure to reach the eggs in the oviduct (Figs. 1 and 2). However, further experiments revealed that the sperm are killed in the uterine cavity in the absence of SVS2 (Fig. 3). Thus, we concluded that the sperm transit through the spermicidal uterine environment from which SVS2 protects the sperm membrane (Fig. 4). In addition, the fertility of sperm that ascend beyond the uterus and the oviduct is strikingly higher than that of the epididymal sperm used for IVF (8), suggesting that sperm are selected in the female reproductive tract. Our finding opens the possibility that a competitive balance between death and survival in the uterus contributes to sperm selection.

In mammals, fertilization is the natural cell transplantation from males to females (19). When cell transplantation is performed for patients, such as those with acute leukemia, transplanted cells are exposed to the immune system of the hosts (20). The immune system in the female reproductive tract is believed to immunologically distinguish the sperm and fetus from pathogens (21). Our results suggest that ejaculated sperm may be treated as foreign objects in the uterus. Because fertilization occurs internally in animals such as mammals, birds, reptiles, and insects (22), the spermicidal system may be conserved in the female reproductive tract of other animals. In fact, in the polyandrous fly (*Scathophaga stercoraria*), sperm viability is significantly lower in

DEVELOPMENTAL BIOLOGY

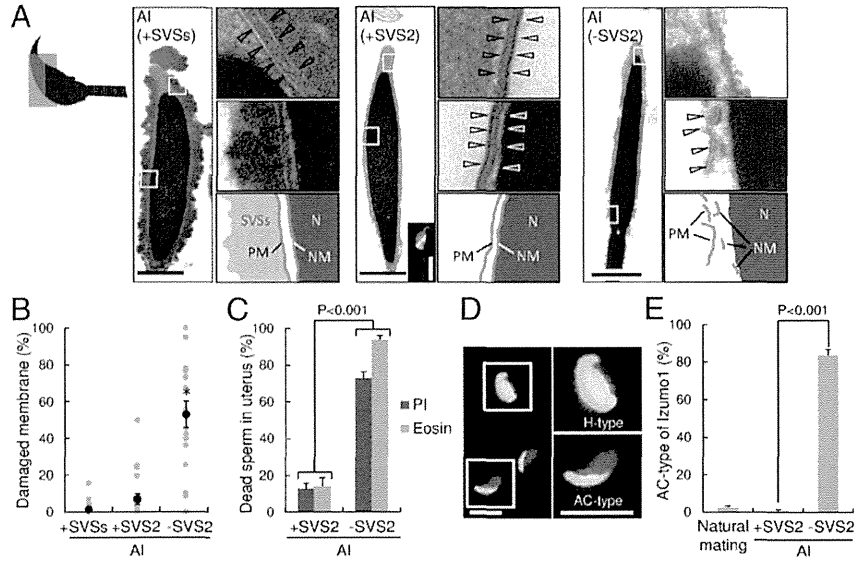

Fig. 3. SVS2-mediated protection of intrauterine sperm from membrane disruption. (*A*) Transmission electron microscopic (TEM) images. Diagram at far left indicates the orientation of sectioned heads of sperm. (*Left*) Sperm with SVSs; (*Center*) sperm with SVS2; (*Right*) sperm without SVS2. (*Left*, *Center*, and *Right*) Right upper and middle images are enlarged views of boxes in the left images, and diagrams are depicted in the right lower images. PM, plasma membrane; N, nucleus; NM, nuclear membrane. (Scale bars: 1 μm.) (*Center*, *Inset*) A fluorescent image of the sperm reacted with anti-SVS2 pAb. (Scale bar, 5 μm.) (*B*) Rates of broken membrane areas in TEM images ($n = 20$). $^*P < 0.001$. (*C*) Rates of dead sperm in the uterus determined by staining with PI and eosin ($n = 3$). (*D*) Fluorescent images of sperm collected from the uterus by staining with anti-IZUMO1 mAb (green) and DAPI (red). (*Right*) Enlarged images of boxes at *Left*. H-type, fusion-capable sperm; AC-type, dead sperm. (Scale bars, 10 μm.) (*E*) Rate of sperm categorized as AC-type ($n = 3$).

the female sperm storage glands immediately after mating than in the male testis (23). If females have the intrinsic ability to kill sexually transmitted pathogens as well as sperm, then males would have had to develop a strategy against such a female spermicidal system. We consider that coevolution of these two systems may select highly specified sperm for fertility.

Cell death is induced in various ways that diverge morphologically and biochemically (24, 25). Cells exposed to natural inducers or cytotoxic substances undergo cell death involving a loss of membrane integrity, which is a hallmark of cell death (26). In animal sperm, the acrosome reaction is an exocytotic event in which membrane fusion takes place between the outer acrosomal membrane and the overlying plasma membrane to form transmembrane pores and allow release or exposure of their contents, resulting in membrane disruption (27). However, the membrane disruption induced by the acrosome reaction completely differs from the membrane disruption caused by cell death, because the integrity of the sperm plasma membrane is maintained throughout and after the acrosome reaction (28). Because the sperm plasma membrane was widely disrupted in the absence of SVS2 (Fig. 3), we concluded that the sperm was dead but not acrosome-reacted.

In mammals, the seminal plasma is mainly secreted from seminal vesicles, the roles of which are discussed mainly with respect to plug formation (29), in addition to other aspects such as energy sources for sperm (30), regulation of sperm motility (31), and preparation of the uterine environment for implantation (21). In polyandrous mating systems, the seminal plasma plays a role in promoting the penetration of self-sperm and eliminating non-self-sperm. For example, the molecular evolution of *SEMG2*, one of the *SVS2* homologs, directly affects the biochemical dynamics of semen coagulation, suppressing fertilization success by copulation with rival males in primates (32). Furthermore, the phenomenon of sperm survival with the aid of the seminal plasma is often found in the animal kingdom, for example in pigs (33) and honey bees (34). Our results provide direct evidence for a molecular mechanism underlying sperm survival whereby the seminal plasma in the uterus protects the sperm. This proposes the concept of "competitive sperm selection" between males and females.

Currently, in cases of male infertility, doctors and patients are often left with few options other than IVF and/or intracytoplasmic sperm injection, mainly owing to the lack of knowledge of in vivo fertilization (35). A recent study revealed that seminal vesicle composition has multiple functions in the female reproductive tract, which not only affect sperm protection and selection before fertilization but also indirectly affect the development and metabolism of progeny (9). The knowledge gained in this and our studies may contribute to the clinical diagnosis of infertility and improve the probability of reproduction. Moreover, taking the functions of SVS2 in the uterus into consideration may lead to the improvement of AI birth rates.

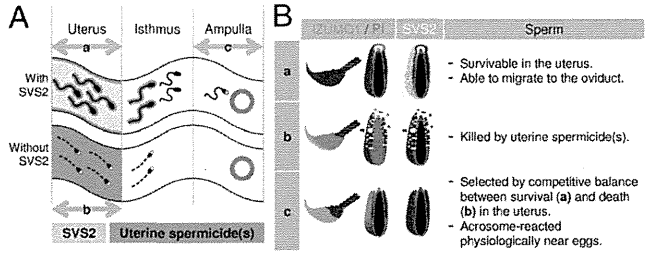

Fig. 4. Schematic model of the role of SVS2 in sperm protection in vivo. (*A*) Sperm migration in the female reproductive tract. Sperm with black heads, acrosome-intact sperm; sperm with white heads, acrosome-reacted sperm. Yellow, SVS2; blue, predicted maternal spermicide(s). a, acrosome-intact sperm penetrated the uterus after natural mating. b, membrane-disrupted dead sperm in the uterus in the absence of SVS2. c, acrosome-reacted sperm penetrated the ampulla. (*B*) Status of acrosomal and plasma membranes of sperm in the female reproductive tract. Categories a, b, and c correspond to those in *A*. Green, sperm membrane stained with anti-IZUMO1 mAb; red, sperm nucleus stained with PI.

Materials and Methods

Antibodies and Chemicals. The mAbs against IZUMO1 and anti-CD46, kindly provided by M. Okabe (Osaka University, Osaka), were used for immunostaining and immunoblotting (18, 36). For immunoblotting, a polyclonal antibody (pAb) was produced in rabbits by immunization with an SVS2 peptide with the following sequence: RKNFNPGNYFTKGGADC (No. SVS2-2). Mouse anti-ADAM3 mAb was purchased from Upstate Biotechnology, and anti-Catsper2 pAb was purchased from Aviva System Biology. Alexa 488-conjugated IgG (Molecular Probes) was used as a secondary antibody. Horseradish peroxidase-conjugated secondary antibodies (Sigma-Aldrich) were used for immunoblotting. Nuclei were counterstained with DAPI (Wako Pure Chemical Industries).

Generation of *SVS2*$^{-/-}$ Mice. Two types of targeting vectors were designed to remove (*i*) whole exons and (*ii*) the portion of the *SVS2* gene spanning exons 1–2 (*SI Appendix*, Fig. S1 *A* and *B*) and were conventionally electroporated into 129/Sv strain-derived ES cells after linearization. Recombinant ES clones were identified by PCR and Southern blot analyses (*SI Appendix*, Fig. S1 *C–F*). Two recombinant ES cell lines (formed by electroporation of each of two kinds of targeting vectors) were microinjected into C57BL/6N strain-derived blastocysts, and the male chimeric mice were obtained. Subsequently, these mice were crossed with C57BL/6N female mice to yield heterozygote offspring. Next, to produce homozygotes, male and female heterozygotes were intercrossed and backcrossed to the C57BL/6N background.

All mice were housed under specific pathogen-free controlled conditions. Food and water were available ad libitum. All animal experiments were performed according to protocols approved by the Institutional Animal Care and Use Committee at the National Institute for Child Health and Development.

Surgical Removal of Accessory Sex Organs. Eight-week-old male ICR mice were anesthetized [2.5% (wt/vol) tribromoethanol, 10 μL/g body weight, intraperitoneally], and depending on the case, either coagulating glands or seminal vesicles were surgically removed via a midventral incision (Fig. 1*D*).

Analysis of Sperm Migration. The sperm location in the female reproductive tract was determined histochemically by hematoxylin and eosin staining. At 3 h after copulation, the female reproductive tract containing the ejaculated sperm was fixed and prepared for paraffin sectioning (thickness, 6 μm). In four parts of the female reproductive tract (vagina, uterus, isthmus, and ampulla of oviduct), the number of sperm head detected at the lumen of each tissue was counted in five consecutive slices. No sperm in the tissue were confirmed by all consecutive slices. Because the oviduct at 3 h after copulation contained ejaculated sperm at greater levels than that at 2 h, we observed the female reproductive tract at 3 h after sperm insemination.

Artificial Insemination. To study the involvement of seminal vesicle secretions in fertilization, sperm were isolated from the epididymides of 8-wk-old male C57BL/6N mice and directly injected into the uterus of 8-wk-old female C57BL/6N mice with a syringe. Before sperm collection the female mice were determined to be in the estrus phase using vaginal smear cytology (37). As depicted in Fig. 2*A* and *SI Appendix*, Fig. S7, a 50-μL aliquot of the epididymal sperm suspension (5×10^7 sperm/mL) was prepared in a yellow tip attached to a 1-mL syringe containing silicon and then injected from the cervix into the uterus with or without the vesicle secretions. The seminal vesicle secretions were surgically collected from one male mouse and dissolved in 1 mL of modified Krebs–Ringer bicarbonate solution (TYH medium), and then centrifuged for 5 min at 10,000 × *g* at room temperature. The supernatant containing soluble proteins from the seminal vesicle was used as SVS and mixed with approximately one-tenth of the volume of the sperm suspension. Silicon was used as a substitute for a copulating plug. Female reproductive tracts from the vagina to oviduct were excised 3 h after sperm injection to allow for sperm migration and for the acrosomal status to be immunocytologically examined. In addition, two-cell embryos and unfertilized eggs were recovered from the oviducts by flushing with TYH medium 24 h after the sperm injection. The numbers of two-cell embryos and unfertilized eggs were counted and used for estimating the success rate of fertilization.

Immunoblotting. The internal fluids were collected from seminal vesicles of male mice and then subjected to Coomassie Brilliant Blue (CBB) staining and immunoblotting as previously described (10). Briefly, the seminal vesicle fluid from one male mouse was diluted in 1 mL of PBS and then solubilized in an equal volume of 2× Laemmli SDS sample buffer. The solubilized samples were resolved by SDS/PAGE on 10% (wt/vol) acrylamide gels and then transferred to Immobilon-FC (Millipore). Mouse seminal vesicle secretion has been reported to consist of up to seven clearly identifiable components, SVS I–VII (38, 39). The detection of immune complexes formed by the proteins of interest and primary antibodies was performed by enzyme-linked color development with horseradish peroxidase conjugated to secondary antibodies. The sperm were collected from the epididymides and also subjected to immunoblotting as described above.

Electron Microscopic Analysis. The sperm were collected from the uterus after AI and then fixed with glutaraldehyde and osmic acid solutions. Ultra-thin sections were prepared as previously described (40). To further quantify the membrane integrity, we measured the length of the damaged membrane per total length of the sperm plasma membrane using Adobe Illustrator CS5 software.

Histochemical Analysis. The male mice were killed, and their testes were examined histochemically by hematoxylin and eosin staining, as described previously (41).

Estimation of Male Fertility in Vivo and in Vitro. To evaluate male fertility in vivo, numbers of pups delivered from 8- to 12-wk-old female mice were recorded after a 2-wk mating period, during which female mice were housed with 8- to 12-wk-old male mice.

For IVF, eggs were collected from superovulated C57BL/6N female mice (8–12 wk old) 14–16 h after human chorionic gonadotropin (hCG) injection (42). The sperm collected from the epididymides of 8- to 12-wk-old male mice were capacitated by incubating in TYH medium for 120 min before insemination. The final concentration of the sperm added to the eggs was 1.5×10^5 sperm/mL.

Detection of Acrosome-Reacted Sperm in the Female Reproductive Tract. To evaluate the acrosomal status of sperm in female reproductive tracts, anti-IZUMO1 mAb and PNA-FITC (Sigma) were used. For immunostaining, sperm were collected from the uterus and fixed for 20 min at 4 °C in a solution containing 4% (wt/vol) paraformaldehyde and 0.1% polyvinylpyrrolidone. After being washed in PBS, sperm were immunostained with anti-IZUMO1 mAb for 1 h at 4 °C and then washed three times in TYH medium, according to previously described methods (42). To further monitor acrosomal status, sperm were collected from the uterus and smeared onto glass slides. Sperm were then air-dried, permeabilized, and fixed with 100% methanol for 10 min at room temperature. After being washed in PBS, sperm were incubated with PNA-FITC in PBS for 10 min at 37 °C and washed three times for 5 min in PBS (10). The fluorescent images were captured by a laser scanning confocal microscope (LSM 510 model; Carl Zeiss Microimaging Inc.). Acrosome-reacted sperm were reacted with anti-IZUMO1 mAb and unreacted with PNA-FITC (10).

To detect acrosome-reacted sperm inside the female reproductive tract, we used transgenic sperm expressing GFP in their acrosomes and RFP in their mitochondria [*B6D2F1-Tg (CAG/su9-DsRed2, Acr3-EGFP) RBGS002Osb*] (14). When the transgenes were introduced into the *SVS2*$^{-/-}$ background, the epididymal acrosome-intact sperm produced in *SVS2*$^{-/-}$ mice could be visualized using dual fluorescence. At 3 h after copulation, the female reproductive tracts containing the ejaculated sperm were fixed and prepared for frozen sections (thickness, 20 μm). In three parts of the female reproductive tract (uterus, isthmus, and ampulla of oviduct), the number of acrosome-reacted sperm (RFP-positive and GFP-negative) was counted and compared with that of acrosome-intact sperm (RFP-positive and GFP-positive).

Measurement of Sperm Motility. For measurement of sperm motility and hyperactivation, CASA operated by IVOS software (Hamilton-Thorne Biosciences) was used, as previously described (42). An aliquot of the capacitated sperm suspension was transferred into a prewarmed counting chamber (depth, 100 mm), and >200 sperm were examined for each sample using standard settings (30 frames acquired at a frame rate of 60 Hz at 37 °C), as previously described. The motility of hyperactivated sperm was determined by using the SORT function of the IVOS software. Sperm were classified as hyperactivated when the trajectory met the following criteria: curvilinear velocity ≥180 μm/s, linearity ≤38%, and amplitude of lateral head displacement ≥9.5 μm.

Generation of BAC Transgenic Mice and Rescue Experiment. A BAC clone (RP23-377B11) containing the full-length mouse *SVS2* gene was purchased from BACPAC Resources Center (Invitrogen) and microinjected into eggs (43). For

the rescue experiment, transgenic mouse lines expressing SVS2 under the control of an *SVS2* native promoter were produced and transferred onto the *SVS2*$^{-/-}$ background.

Detection of the Spermicidal Effect of UF. To evaluate the percentage of dead sperm influenced by UF, the epididymal sperm without SVS2 were incubated in TYH medium containing 10% (vol/vol) UF and oviductal fluid for 3 h and then stained with both 10 μg/mL PI (Sigma) and 10 μg/mL Hoechst 33342 (Invitrogen). After estrus phase was determined by vaginal smear cytology (37), the UF was collected from each of the uterine horns of 8- to 10-wk-old C57BL/6N female mice using a micropipette. The oviductal fluid was collected from the ampulla of oviduct in superovulated C57BL/6N female mice 14–16 h after hCG injection. For each sample, after >200 sperm were examined, doubly PI- and Hoechst 33342-positive sperm were counted as dead sperm, whereas only Hoechst 33342-positive sperm were counted as living sperm.

Statistical Analysis. Comparisons were made using one-way analysis of variance following Scheffé's method, the Mann-Whitney *U* test, or Fisher's exact test. Statistical significance was defined as $P < 0.05$. Results are expressed as the mean ± SEM.

ACKNOWLEDGMENTS. We thank M. Okabe for providing the anti-IZUMO1 mAb, as well as M. Morisawa, T. Iwamoto, and N. Inoue for critical discussions. This work was supported by a grant from the Ministry of Health, Labor and Welfare, and a grant-in-aid for scientific research from the Ministry of Education, Culture, Sports, and Technology of Japan.

1. Suarez SS (2006) in *Knobil and Neill's Physiology of Reproduction*, ed Neill JD (Academic, New York), 3rd Ed, pp 113–145.
2. Chang MC (1957) A detrimental effect of seminal plasma on the fertilizing capacity of sperm. *Nature* 179(4553):258–259.
3. Bedford JM, Chang MC (1962) Removal of decapacitation factor from seminal plasma by high-speed centrifugation. *Am J Physiol* 202(1):179–181.
4. Fraser LR (1984) Mouse sperm capacitation in vitro involves loss of a surface-associated inhibitory component. *J Reprod Fertil* 72(2):373–384.
5. Nixon B, et al. (2006) The identification of mouse sperm-surface-associated proteins and characterization of their ability to act as decapacitation factors. *Biol Reprod* 74(2): 275–287.
6. Lu CH, et al. (2011) SERPINE2, a serine protease inhibitor extensively expressed in adult male mouse reproductive tissues, may serve as a murine sperm decapacitation factor. *Biol Reprod* 84(3):514–525.
7. Fukami K, et al. (2001) Requirement of phospholipase Cdelta4 for the zona pellucida-induced acrosome reaction. *Science* 292(5518):920–923.
8. Suarez SS, Pacey AA (2006) Sperm transport in the female reproductive tract. *Hum Reprod Update* 12(1):23–37.
9. Bromfield JJ, et al. (2014) Maternal tract factors contribute to paternal seminal fluid impact on metabolic phenotype in offspring. *Proc Natl Acad Sci USA* 111(6): 2200–2205.
10. Kawano N, Yoshida M (2007) Semen-coagulating protein, SVS2, in mouse seminal plasma controls sperm fertility. *Biol Reprod* 76(3):353–361.
11. Kawano N, Yoshida K, Iwamoto T, Yoshida M (2008) Ganglioside GM1 mediates decapacitation effects of SVS2 on murine spermatozoa. *Biol Reprod* 79(6):1153–1159.
12. Olson EN, Arnold HH, Rigby PW, Wold BJ (1996) Know your neighbors: Three phenotypes in null mutants of the myogenic bHLH gene MRF4. *Cell* 85(1):1–4.
13. Dean MD (2013) Genetic disruption of the copulatory plug in mice leads to severely reduced fertility. *PLoS Genet* 9(1):e1003185.
14. Hasuwa H, et al. (2010) Transgenic mouse sperm that have green acrosome and red mitochondria allow visualization of sperm and their acrosome reaction in vivo. *Exp Anim* 59(1):105–107.
15. Graham JK, Kunze E, Hammerstedt RH (1990) Analysis of sperm cell viability, acrosomal integrity, and mitochondrial function using flow cytometry. *Biol Reprod* 43(1): 55–64.
16. Emoto K, et al. (1996) Redistribution of phosphatidylethanolamine at the cleavage furrow of dividing cells during cytokinesis. *Proc Natl Acad Sci USA* 93(23): 12867–12872.
17. Satouh Y, Inoue N, Ikawa M, Okabe M (2012) Visualization of the moment of mouse sperm-egg fusion and dynamic localization of IZUMO1. *J Cell Sci* 125(Pt 21): 4985–4990.
18. Inoue N, et al. (2003) Disruption of mouse CD46 causes an accelerated spontaneous acrosome reaction in sperm. *Mol Cell Biol* 23(7):2614–2622.
19. Ikawa M, Inoue N, Benham AM, Okabe M (2010) Fertilization: A sperm's journey to and interaction with the oocyte. *J Clin Invest* 120(4):984–994.
20. Thomas ED, et al. (1977) One hundred patients with acute leukemia treated by chemotherapy, total body irradiation, and allogeneic marrow transplantation. *Blood* 49(4):511–533.
21. Schuberth HJ, et al. (2008) Immunological responses to semen in the female genital tract. *Theriogenology* 70(8):1174–1181.
22. Snook RR, Hosken DJ, Karr TL (2011) The biology and evolution of polyspermy: insights from cellular and functional studies of sperm and centrosomal behavior in the fertilized egg. *Reproduction* 142(6):779–792.
23. Bernasconi G, Hellriegel B, Heyland A, Ward PI (2002) Sperm survival in the female reproductive tract in the fly *Scathophaga stercoraria* (L.). *J Insect Physiol* 48(2): 197–203.
24. Elmore S (2007) Apoptosis: A review of programmed cell death. *Toxicol Pathol* 35(4): 495–516.
25. Orrenius S, Nicotera P, Zhivotovsky B (2011) Cell death mechanisms and their implications in toxicology. *Toxicol Sci* 119(1):3–19.
26. McNeil PL, Steinhardt RA (1997) Loss, restoration, and maintenance of plasma membrane integrity. *J Cell Biol* 137(1):1–4.
27. Toshimori K (2009) Dynamics of the mammalian sperm head: Modifications and maturation events from spermatogenesis to egg activation. *Adv Anat Embryol Cell Biol* 204:5–94.
28. Uto N, Yoshimatsu N, Lopata A, Yanagimachi R (1988) Zona-induced acrosome reaction of hamster spermatozoa. *J Exp Zool* 248(1):113–120.
29. Mann T, Lutwak-Mann C (1981) *Male Reproductive Function and Semen* (Springer, Berlin).
30. Mann T, Lutwak-Mann C (1948) Studies on the metabolism of semen. 4. Aerobic and anaerobic utilization of fructose by spermatozoa and seminal vesicles. *Biochem J* 43(2):266–270.
31. Luo CW, Lin HJ, Chen YH (2001) A novel heat-labile phospholipid-binding protein, SVS VII, in mouse seminal vesicle as a sperm motility enhancer. *J Biol Chem* 276(10): 6913–6921.
32. Dorus S, Evans PD, Wyckoff GJ, Choi SS, Lahn BT (2004) Rate of molecular evolution of the seminal protein gene SEMG2 correlates with levels of female promiscuity. *Nat Genet* 36(12):1326–1329.
33. Rozeboom KJ, Troedsson MH, Hodson HH, Shurson GC, Crabo BG (2000) The importance of seminal plasma on the fertility of subsequent artificial inseminations in swine. *J Anim Sci* 78(2):443–448.
34. King M, Eubel H, Millar AH, Baer B (2011) Proteins within the seminal fluid are crucial to keep sperm viable in the honeybee *Apis mellifera*. *J Insect Physiol* 57(3):409–414.
35. Hansen M, Bower C, Milne E, de Klerk N, Kurinczuk JJ (2005) Assisted reproductive technologies and the risk of birth defects—a systematic review. *Hum Reprod* 20(2): 328–338.
36. Inoue N, Ikawa M, Isotani A, Okabe M (2005) The immunoglobulin superfamily protein Izumo is required for sperm to fuse with eggs. *Nature* 434(7030):234–238.
37. Gurtovenko AA, Vattulainen I (2007) Lipid transmembrane asymmetry and intrinsic membrane potential: Two sides of the same coin. *J Am Chem Soc* 129(17):5358–5359.
38. Chen YH, Pentecost BT, McLachlan JA, Teng CT (1987) The androgen-dependent mouse seminal vesicle secretory protein IV: Characterization and complementary deoxyribonucleic acid cloning. *Mol Endocrinol* 1(10):707–716.
39. Fawell SE, McDonald CJ, Higgins SJ (1987) Comparison of seminal vesicle secretory proteins of rodents using antibody and nucleotide probes. *Mol Cell Endocrinol* 50(1-2):107–114.
40. Iuchi Y, et al. (2009) Peroxiredoxin 4 knockout results in elevated spermatogenic cell death via oxidative stress. *Biochem J* 419(1):149–158.
41. Papaioannou MD, et al. (2009) Sertoli cell Dicer is essential for spermatogenesis in mice. *Dev Biol* 326(1):250–259.
42. Kawano N, et al. (2010) Mice lacking two sperm serine proteases, ACR and PRSS21, are subfertile, but the mutant sperm are infertile in vitro. *Biol Reprod* 83(3):359–369.
43. Antoch MP, et al. (1997) Functional identification of the mouse circadian Clock gene by transgenic BAC rescue. *Cell* 89(4):655–667.

TBX1 Mutation Identified by Exome Sequencing in a Japanese Family with 22q11.2 Deletion Syndrome-Like Craniofacial Features and Hypocalcemia

Tsutomu Ogata[1*9], Tetsuya Niihori[2,9], Noriko Tanaka[3,9], Masahiko Kawai[4], Takeshi Nagashima[5], Ryo Funayama[5], Keiko Nakayama[5], Shinichi Nakashima[1], Fumiko Kato[1], Maki Fukami[6], Yoko Aoki[2], Yoichi Matsubara[2,6]

1 Department of Pediatrics, Hamamatsu University School of Medicine, Hamamatsu, Japan, **2** Department of Medical Genetics, Tohoku University School of Medicine, Sendai, Japan, **3** Department of Pediatrics, Kurashiki Central Hospital, Kurashiki, Japan, **4** Department of Pediatrics, Kyoto University School of Medicine, Kyoto, Japan, **5** Division of Cell Proliferation, United Centers for Advanced Research and Translational Medicine, Tohoku University Graduate School of Medicine, Sendai, Japan, **6** National Research Institute for Child Health and Development, Tokyo, Japan

Abstract

Background: Although *TBX1* mutations have been identified in patients with 22q11.2 deletion syndrome (22q11.2DS)-like phenotypes including characteristic craniofacial features, cardiovascular anomalies, hypoparathyroidism, and thymic hypoplasia, the frequency of *TBX1* mutations remains rare in deletion-negative patients. Thus, it would be reasonable to perform a comprehensive genetic analysis in deletion-negative patients with 22q11.2DS-like phenotypes.

Methodology/Principal Findings: We studied three subjects with craniofacial features and hypocalcemia (group 1), two subjects with craniofacial features alone (group 2), and three subjects with normal phenotype within a single Japanese family. Fluorescence *in situ* hybridization analysis excluded chromosome 22q11.2 deletion, and genomewide array comparative genomic hybridization analysis revealed no copy number change specific to group 1 or groups 1+2. However, exome sequencing identified a heterozygous *TBX1* frameshift mutation (c.1253delA, p.Y418fsX459) specific to groups 1+2, as well as six missense variants and two in-frame microdeletions specific to groups 1+2 and two missense variants specific to group 1. The *TBX1* mutation resided at exon 9C and was predicted to produce a non-functional truncated protein missing the nuclear localization signal and most of the transactivation domain.

Conclusions/Significance: Clinical features in groups 1+2 are well explained by the *TBX1* mutation, while the clinical effects of the remaining variants are largely unknown. Thus, the results exemplify the usefulness of exome sequencing in the identification of disease-causing mutations in familial disorders. Furthermore, the results, in conjunction with the previous data, imply that *TBX1* isoform C is the biologically essential variant and that *TBX1* mutations are associated with a wide phenotypic spectrum, including most of 22q11.2DS phenotypes.

Citation: Ogata T, Niihori T, Tanaka N, Kawai M, Nagashima T, et al. (2014) *TBX1* Mutation Identified by Exome Sequencing in a Japanese Family with 22q11.2 Deletion Syndrome-Like Craniofacial Features and Hypocalcemia. PLoS ONE 9(3): e91598. doi:10.1371/journal.pone.0091598

Editor: Reiner Albert Veitia, Institut Jacques Monod, France

Received November 12, 2013; **Accepted** February 12, 2014; **Published** March 17, 2014

Funding: This work was supported in part by grants from the Ministry of Health, Labor, and Welfare, from the Ministry of Education, Culture, Sports, Science and Technology, and from the National Center for Child Health and Development. The funders had no role in study design, data collection and analysis, decision to publish, or preparation of the manuscript.

Competing Interests: The authors have declared that no competing interests exist.

* E-mail: tomogata@hama-med.ac.jp

9 These authors contributed equally to this work.

Introduction

Chromosome 22q11.2 deletion syndrome (22q11.2DS) is a developmental disorder associated with characteristic craniofacial features with velopharyngeal incompetence, cardiovascular anomalies primarily affecting the outflow tracts, hypoparathyroidism and resultant hypocalcemia, and thymic hypoplasia leading to susceptibility to infection [1]. This condition is also frequently accompanied by non-specific clinical features such as developmental retardation [1]. Expressivity and penetrance of these features are highly variable and, consistent with this, chromosome 22q11.2 deletions have been identified in DiGeorge syndrome (DGS) and velocardiofacial syndrome (VCFS) with overlapping but different patterns of clinical features [1].

While multiple genes are involved in chromosome 22q11.2 deletions [2], *TBX1* (T-box 1) has been regarded as the major gene relevant to the development of clinical features in 22q11.2DS [3]. Indeed, heterozygous *TBX1* mutations have been identified in several deletion-negative patients with 22q11.2DS phenotype [2–8], and mouse studies argue for the critical role of *Tbx1* in the development of 22q11.2DS phenotypes [3]. However, the frequency of *TBX1* mutations remains rare in deletion-negative patients: Gong et al. identified only a few probable *TBX1* mutations after studying 40 patients with DGS/VCFS phenotypes

[4], and Zweier et al. found a single *TBX1* mutation after examining 10 patients with 22q11.2DS phenotype [8]. This indicates the presence of genetic heterogeneity in the development of 22q11.2DS phenotype in deletion-negative patients. Consistent with this, another DGS/VCFS locus has been assigned to chromosome 10p13-14 region [9]. Thus, it would be reasonable to perform a comprehensive genetic analysis in deletion-negative patients with 22q11.2DS phenotype.

In this regard, recent advance in molecular technologies has enabled to perform comprehensive genetic analyses, thereby contributing to the identification of underlying factors in genetic disorders. Indeed, genomewide array comparative genomic hybridization (CGH) has identified multiple disease-associated copy-number changes [10], and exome sequencing has discovered multiple disease-causing gene mutations [11]. In particular, these technologies can be powerful methods for familial disorders, because it is predicted that a single copy-number change or mutation is shared in common by affected subjects and is absent from non-affected subjects within a family.

Here, we performed array CGH analysis and exome sequencing in a family with 22q11.2DS-like clinical features. Although this study did not discover a novel disease gene, a *TBX1* mutation was successfully identified.

Materials and Methods

Ethics statement

The Institutional Review Board Committees of Hamamatsu University School of Medicine, Tohoku University School of Medicine, Kurashiki Central Hospital, and National Research Institute for Child Health and Development considered and approved the study, consent/assent procedures, and the publication of images and case details associated with this work. The individuals in this manuscript have given written informed consent (as outlined in PLOS consent form) to publish these case details. Actually, this study was performed after obtaining written informed consent from the parents of the child subjects and from the adult subjects. Furthermore, the mother and the elder brother aged 19 years old have given written informed consent to publication of the facial photographs of the two brothers; in addition, the younger brother aged 10 years has given informed assent.

Clinical Report

The pedigree of this Japanese family is shown in Fig. 1, and clinical findings of the family members are summarized in Table 1. The proband (subject III-5) was found to have hypocalcemia and hyperphosphatemia in a pre-operation laboratory test for repeated otitis media at 8 years of age, and was referred to Department of Pediatrics at Kurashiki Central Hospital. Subsequent examination revealed borderline low serum intact PTH value. Thus, he was diagnosed as having hypoparathyroidism, and received vitamin D therapy. Furthermore, physical examination showed characteristic craniofacial features with velopharyngeal incompetence suggestive of 22q11.2DS.

Similar craniofacial features were also exhibited by subjects II-2, III-1, III-6, and III-7, and hypocalcemia was also identified in subjects II-2 and III-7. Actually, subject II-2 was taking vitamin D, and subject III-7 was noticed to have hypocalcemia at birth because of the history of subject III-5, and was treated with vitamin D. The five subjects with 22q11.2DS-like craniofacial features lacked cardiovascular anomalies; while they also lacked susceptibility to infection, except for repeated otitis media in subject III-5, thymic hypoplasia was not evaluated in four of the five subjects. By contrast, the five subjects exhibited borderline to mild developmental delay. Indeed, adult subjects II-2 and III-1 had some difficulty in verbal communications, although they were able to get on their daily life, and subject II-2 was able to take care of family members. Similarly, child subjects III-5, III-6, and III-7 also showed speech delay, and subjects III-5 and III-7 received speech therapy. Furthermore, subject III-7 was diagnosed as having pervasive developmental disorder, and his verbal, performance, and full scale intelligence quotients were assessed as 63, 64, and 60, respectively, by the WISC-III method at 10 years of age. In addition, subject II-2 had sensorineural deafness, and subject III-5 had Graves' disease.

Molecularly Studied Subjects

Molecular studies were performed for eight subjects in this family, using peripheral blood samples. They were divided into three groups in terms of clinical findings: group 1, subjects II-2, III-5, and III-7 with craniofacial features and hypocalcemia; group 2, subjects III-1 and III-6 with craniofacial features alone; and group 3, subjects II-1, III-3, and IV-1 with apparently normal phenotype (Fig. 1).

FISH and Array CGH Analyses

Fluorescence *in situ* hybridization (FISH) analysis was performed with a probe for *HIRA* on the commonly deleted chromosome 22q11.2 region and that for *ARSA* at chromosome 22q13 utilized as an internal control (Abott). Array CGH was carried out using a genomewide 2x400K Agilent platform catalog array, according to the manufacturer's instructions (Agilent Technologies), and copy number variants/polymorphisms were screened with Agilent Genomic Workbench software using the Database of Genomic Variants (http://dgv.tcag.ca/dgv/app/home).

Exome and Sanger Sequencings

Exon capture was performed with the SureSelect Human All Exon kit v4 (Agilent Technologies). Exon libraries were sequenced with the Illumina Hiseq 2000 platform according to the manufacturer's instructions (Illumina), providing 108–122 average depth for each sample. Paired 101-base pair reads were aligned to the reference human genome (UCSChg19) using the Burrows-Wheeler Alignment tool [12]. Likely PCR duplicates were removed with the Picard program (http://picard.sourceforge.net/). Single-nucleotide variants and indels were identified using the Genome Analysis Tool Kit (GATK) v1.6 software [13]. SNVs and indels were annotated against the RefSeq database, 1000 Genomes Project variant data, and dbSNP135 with the ANNOVAR program [14].

To confirm mutations indicated by exome sequencing, Sanger sequencing was performed for PCR products obtained with primers flanking the detected mutations, using a 3500xL genetic analyzer (Life Technologies). Furthermore, the PCR products were subcloned with TOPO TA Cloning Kit (Life Technologies), and normal and mutant alleles were sequenced separately.

In silico protein functional analysis

Function of proteins with missense variations was assessed by Polymorphism Phenotyping-2 (PolyPhen-2, http://genetics.bwh.harvard.edu/pph2/) and Sorting Intolerant From Tolerant (SIFT, http://sift.jcvi.org/), and that of proteins with in-frame amino acid deletions was evaluated by PROVEAN predictions (http://provean.jcvi.org/index.php).

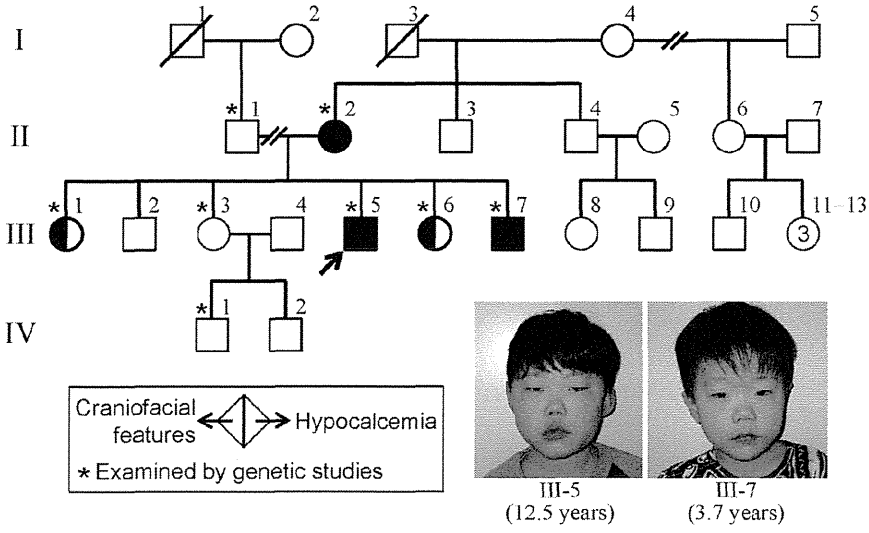

Figure 1. The pedigree of this family. Facial features of subjects III-5 and III-7 are shown.
doi:10.1371/journal.pone.0091598.g001

Results

FISH and Array CGH Analyses

FISH analysis delineated two signals for *HIRA* (Fig. 2A). Array CGH analysis revealed no copy number change specific to group 1 or groups 1+2, in the entire genome including chromosome 10p13-14 and chromosome 22q11.2 regions (Fig. 2B).

Exome and Sanger Sequencings

Exome sequencing identified nine heterozygous non-synonymous variants (six missense variants, two in-frame microdeletions, and one frameshift variant) that were specific to groups 1+2 (namely, they were present in groups 1+2 and absent from group 3 as well as from 1000 Genomes, dbSNP135, and our in-house exome data from 70 individuals) (Table S1). Notably, the frameshift variant (c.1253delA, p.Y418fsX459) was found at exon 9C of *TBX1* for DGS/VCFS (Fig. 3). Of the remaining eight variants, two variants were also detected in disease-related genes: p.G204R in *HDAC4* for brachydactyly-mental retardation syndrome [15], and p.276del in *CCND1* constituting a susceptibility factor for colorectal cancer and a modifier for von Hippel-Lindau disease [16,17]. Exome sequencing also detected two heterozygous missense variants that were specific to group 1 (Table S1).

When all variants were included, exome sequencing revealed: (1) 83 non-synonymous and 86 synonymous variants that were present in groups 1+2 and absent from group 3 (Table S2); (2) 54 non-synonymous and 48 synonymous variants that were present in group 1 and absent from groups 2+3 (Table S3); (3) 6,033 non-synonymous and 6,667 synonymous variants that were present in groups 1+2, but not specific to groups 1+2 (thus, they may be present in group 3 or absent from group 3); and (4) 7,073 non-synonymous and 7,861 synonymous variants that were present in group 1, but not specific to group 1. Furthermore, comparison of the exome sequencing data between group 1 with hypocalcemia and group 2 without hypocalcemia revealed 231 non-synonymous and 254 synonymous variants that were present in group 1 and absent from group 2 (Table S4), and 246 non-synonymous and 242 synonymous variants that were present in group 2 and absent from group 1 (Table S5). (The variant data other than those described in Supplemental Tables may be available on request after discussion with the family members and approval by our IRBs, because they contain a huge amount of individual genetic information.)

In silico protein functional analysis

The results are summarized in Table S1. The p.G204R in *HDAC4* and the p.E276del in *CCND1* were assessed as non-pathologic, while some variants were evaluated as potentially pathologic.

Discussion

Exome sequencing successfully identified a heterozygous frameshift variant on exon 9C of *TBX1*. The c.1253delA (p.Y418fsX459) appears to be a disease-causing mutation, because it is predicted that this variant escapes nonsense-mediated mRNA decay due to its position on the final exon [18] and produces a truncated protein lacking the nuclear localization signal (NLS) and most of the transactivation domain (TAD) on exon 9C (Fig. 3) [19]. In support of this, functional studies for a similar c.1223delC (p.S408fsX459) mutation on exon 9C have shown that the truncated p.S408fsX459 protein was incapable of localizing to nucleus and lost transactivation function [2,5,19]. One may argue that this c.1253delA mutation affects *TBX1* isoform C (*TBX1C*, TBX1-003) alone, while *TBX1* produces three transcript variants containing T-box [2,4] (Fig. 3). However, *TBX1C* is the major transcript with the NLS and the TAD in human and is highly homologous to mouse *Tbx1* [4] (Fig. S1).

Craniofacial features in groups 1+2 and hypocalcemia in group 1 are well explained by the *TBX1* mutation [3]. This argues for a critical role of this mutation in the phenotypic development in groups 1+2, while the clinical effects of the remaining variants identified by exome sequencing are largely unknown. In this regard, comparison between group 1 with hypocalcemia and group 2 without hypocalcemia revealed a large number of non-synonymous and synonymous variants that exclusively belonged to either group 1 (Table S4) or group 2 (Table S5), although the lists did not contain a c.2968A>G (p.R990G) SNP in *CASR* (calcium sensing receptor) that has a gain-of-function effect and appears to raise the susceptibility to hypocalcemia (Fig. S2) [20]. Thus, it is

Table 1. Clinical findings of the family members.

	TBX1 mutation (+)					*TBX1* mutation (−)			*TBX1* mutation (N.E.)		
Individual	**II-2**	**III-1**	**III-5**	**III-6**	**III-7**	**II-1**	**III-3**	**IV-1**	**II-3**	**II-4**	**III-2**
Present age (year)	51	26	19	13	10	59	22	5	50	49	25
Sex	F	F	M	F	M	M	F	M	M	M	M
Craniofacial features	+	+	+	+	+	−	−	−	−	−	−
Hypertelorism	+	+	+	+	+	−	−	−	−	−	−
Blepharophimosis	+	+	+	+	+	−	−	−	−	−	−
Low set ears	+	+	+	+	+	−	−	−	−	−	−
Auricular anomalies	+	−	−	−	−	−	−	−	−	−	−
Narrow nose	+	+	+	+	+	−	−	−	−	−	−
Cleft palate	−	−	−	−	−	−	−	−	−	−	−
Micrognathia	±	+	+	+	+	−	−	−	−	−	−
Velopharyngeal incompetence	+[d]	+	+	+	+	−	−	−	−	−	−
Hypoparathyroidism	+	−	+	−	+	−	−	−	−	−	−
Age at examination (year)	44	17	8	4	0 (1 day)	N.E.	15	0 (6 days)	N.E.	N.E.	18
Serum calcium (mg/dL)[a]	7.6[e]	9.0	6.0	9.1	5.9	…	9.0	9.8	…	…	9.6
Serum i-phosphate (mg/dL)[a]	3.9[e]	4.9	9.1	5.0	N.E.	…	4.8	6.3	…	…	4.6
Serum intact PTH (pg/dL)[a]	31[e]	N.E.	15	N.E.	19	…	N.E.	34	…	…	N.E.
Cardiovascular anomalies[b]	−	−	−	−	−	−	−	−	−	−	−
Hypoplastic thymus[c]	−	N.E.	N.E.	N.E.	N.E.	N.E.	N.E.	N.E.	N.E.	N.E.	N.E.
Susceptible to infection	−	−	−[f]	−	−	−	−	−	−	−	−
Other features	−	−	−	−	−	−	−	−	−	−	−
Developmental retardation	+	+	+[g]	+	+[g]	−	−	−	−	−	−
Sensorineural deafness	+[h]	−	−	−	−	−	−	−	−	−	−
Graves' disease	−	−	+[i]	−	−	−	−	−	−	−	−

Individuals correspond to those shown in Fig. 1.
i-phosphate: inorganic phosphate; SD: standard deviation; F: female; M: male; and N.E.: not examined.
[a]Reference values: calcium, 9.0–11.0 mg/dL in infants and 8.8–10.2 mg/dL in adults; inorganic phosphate, 4.8–7.5 mg/dL in infants and 2.5–4.5 mg/dL in adults, and intact PTH, 10–65 pg/dL in infants and 14–55 pg/dL in adults.
Conversion factor to the SI unit: 0.25 for calcium (mmol/L), 0.32 for inorganic phosphate (mmol/L), and 0.106 for intact PTH (pmol/L).
[b]Examined by echocardiography, chest roentgenography, and/or electrocardiography.
[c]Examined by computed tomography.
[d]Received velopharyngeal closure.
[e]On treatment with vitamin D.
[f]Repeated otitis media only.
[g]Received speech therapy.
[h]Required hearing aids.
[i]At the time of diagnosis (11 years of age), serum TSH was <0.01 mIU/L, free T_3 33.1 pg/mL [51.0 pmol/L], free T_4 5.11 ng/dL [65.8 nmol/L], and TSH receptor antibody 1284% [normal range <1.9%].
doi:10.1371/journal.pone.0091598.t001

likely that, together with environmental factors, the combination of hitherto unknown calcium metabolism-related functional variants would underlie different serum calcium values between groups 1 and 2.

In addition to craniofacial features with and without hypocalcemia, *TBX1* mutation positive subject II-2 had sensorineural deafness, and III-5 had Graves' disease. Since such features are occasionally manifested by patients with 22q11.2DS [21,22], the results may suggest the relevance of *TBX1* to such rather infrequent features in 22q11.2DS.

The five *TBX1* mutation positive subjects in groups 1+2 lacked cardiovascular lesion and manifested borderline to mild developmental retardation (while they had no susceptibility to infection, assessment of thymic hypoplasia remained fragmentary). By contrast, cardiovascular lesion is frequently observed and developmental retardation is rare in previously reported patients with *TBX1* mutations, although clinical features are fairly variable among mutation positive patients (Table 2). Such difference would more or less be ascribed to an examination bias that *TBX1* has been analyzed in patients with isolated cardiovascular lesion in several studies [4,6,7] or to the functional difference of the mutant proteins [2,5–8]. However, in seven patients who have been examined for DGS/VCFS-like clinical features and found to have frameshift mutations on exon 9C (p.S408fsX459, p.H425fsX613, and p.S431fsX608) affecting the NLS and the TAD, cardiovascular lesion was present in four patients and developmental delay was absent or not described, despite apparent similarity in the ascertainment of patients and the function of mutant proteins between the seven patients and the five affected subjects in this family (Table 2) [2–5].

Thus, there may be protective factor(s) for cardiovascular lesion and susceptibility factor(s) for developmental delay in groups 1+2.

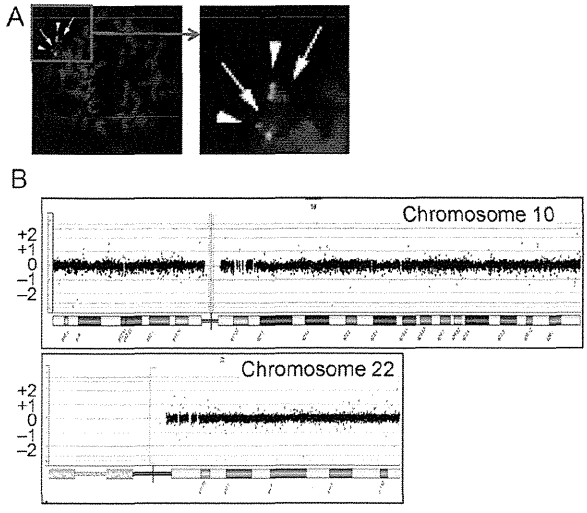

Figure 2. FISH and array CGH analyses in the proband (III-5). A. FISH analysis. Two signals are shown for both *HIRA* at 22q11.2 (red signals indicated by arrows) and *ARSA* at 22q13 (green signals indicated by arrowheads). **B.** Array CGH analysis. No copy number change is found for chromosome 10 carrying the second DiGeorge region and chromosome 22 harboring the DGS/VCFS critical region, as well as other chromosomes (not shown). Black, red, and green dots denote signals indicative of the normal, the increased (>+0.5), and the decreased (<−0.8) copy numbers, respectively. Although several red and green signals are seen, there is no portion associated with ≥3 consecutive red or green signals.
doi:10.1371/journal.pone.0091598.g002

In this regard, a simple explanation would be that protective factor(s) for cardiovascular lesion are present in groups 1+2 and may be present in group 3 or absent from group 3, whereas susceptibility factor(s) for developmental delay is present in groups 1+2 and absent from group 3. Since 6,033 non-synonymous and 6,667 synonymous variants were found to be present in groups 1+2 but not specific to groups 1+2, and 83 non-synonymous and 86 synonymous variants were revealed to be present in groups 1+2 and absent from group 3, a certain fraction of functional variants may constitute protective factor(s) for cardiovascular lesion and susceptibility factor(s) for developmental delay. In addition, while p.G204R on *HDAC4* for brachydactyly-mental retardation syndrome was assessed as non-pathologic by *in silico* analysis, it may have played a certain role in the occurrence of developmental delay in groups 1+2. Actually, such protective and susceptibility factor(s) would be more complex, with the effects of functional variants unique to each patient as well as the influences of environmental factors. Furthermore, it remains possible that the c.1253delA (p.Y418fsX459) mutation found in this study may be related to a specific phenotype characterized by the presence of craniofacial features and developmental delay and by the absence of cardiovascular lesion, because of a hitherto unrevealed mechanism(s). This matter awaits further studies.

Besides the clinical findings, several matters are also notable in the nine apparently pathologic *TBX1* mutations identified to date (Table 2). First, the mutations reside on exons 3–8 common to isoforms A–C or on exon 9C specific to isoform C, with no mutation on exons 9A and 9B specific to isoforms A and B. This would be consistent with *TBX1C* having the primary biological function. Second, while most mutations have loss-of-function effects, gain-of-function effects have been suggested for p.F148Y, p.H194Q, and p.310S by *in vitro* studies [8]. Thus, *TBX1* loss-of-function mutations and gain-of-function mutations may result in overlapping clinical features. Lastly, the c.1274_1281delACTATCTC (p.H425fsX613) missing the NLS on exon 9C was shared by a patient with DGS-like phenotype and the apparently normal mother, and the c.129_185del57 (p.43-61del19) with reduced transcriptional activity was common to a patient with non-syndromic tetralogy of Fallot and the apparently normal mother. This would imply the reduced penetrance of phenotypes caused by these mutations.

In summary, we identified a *TBX1* mutation by exome sequencing in a family with chromosome 22q11.2 deletion-like

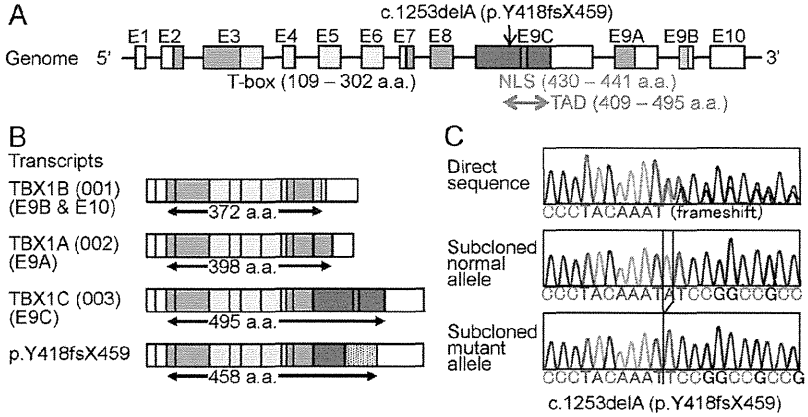

Figure 3. *TBX1* mutation identified in this family. A. Genomic structure of *TBX1* and the position of the mutation. The color and the white boxes represent the coding regions and the untranslated regions on exons 1–10 (E1–E10), respectively; the red, the purple, and the orange segments indicate the coding regions on the final exons 9C, 9A, and 9B (splice variants), respectively. The T-box is indicated by yellow boxes, the nuclear localization signal (NLA) by a blue segment, and the transactivation domain (TAD) by a green arrow. The c.1253delA (p.Y418fsX459) identified in this family resides on exon 9C. **B.** Transcripts of *TBX1*. Three variants are formed by alternative splicing of the final exons 9C, 9A, and 9B. The c.1253delA (p.Y418fsX459) mutation is predicted to yield a truncated TBX1C protein missing the NLS and most of the TAD. The stippled box of p.Y418fsX459 denotes aberrant amino acid sequence produced by the frameshift mutation. **C.** Electrochromatograms showing the frameshift mutation by Sanger sequencing. The primer sequences used are: 5′-GCGGCCAAGAGCCTTCTCT-3′ and 5′-GGGTGGTAGCCGTGGCCA-3′.
doi:10.1371/journal.pone.0091598.g003

Table 2. Summary of patients with *TBX1* mutations.

	TBX1C only					TBX1A–C				22q11.2DS
Position	**Exon 9C**	**Exon 9C**	**Exon 9C**	**Exon 9C**	**Exon 9C**	**Exon 3**	**Exon 4**	**Exon 5**	**Exon 8**	
cDNA change[a]	c.1223	c.1253	c.1274_1281	c.1293_1315	c.1399_1428	c.129_185	c.443T>A	c.582C>G	c.928G>A	Deletion
	delC	delA	del8	del23[h]	dup30[k]	del57[k]				
Amino acid	p.S408	p.Y418	p.H425	p.S431	p.467_476	p.43_61	p.F148Y	p.H194Q	p.G310S	
change	fsX459	fsX459	fsX613	fsX608	dup10A	del19				
NLS (exon 9C)	–	–	–	+[i]	+[i]	+	+	+	+	
TAD (exon 9C)	–	Involved	Involved	Involved	Involved	+	+	+	+	
Function	LOF	N.E.	N.E.	LOF	LOF	Reduced	GOF[m]	GOF[m]	GOF[m]	
Patient number	3	5	1	3[j]	2	1	1	2	1	558
Occurrence	Familial	Familial	Sporadic[g]	Familial	Sporadic	Sporadic[g]	Sporadic	Familial	Sporadic	
Facial features[b]	3/3	5/5	+	3/3	0/2	–	+	2/2	+	100%
Nasal voice[c]	2/3	5/5	N.D.	3/3	0/2	–	+	0/2	+	32%
Cardiovascular anomalies	1/3	0/5	+	2/3	2/2	+	+	0/2	+	57%
Hypopara-thyroidism[d]	1/3	3/5	+	N.D.	0/2	–	–	0/2	+	60%
Hypoplastic thymus	1/2[e]	0/1[f]	+	N.D.	0/2	–	–	N.E.	+	?
Susceptible to infection	N.D.	0/5	N.D.	N.D.	0/2	–	N.D.	N.D.	N.D.	?
Developmental retardation	0/3	5/5	N.D	0/3	0/2	–	–	1/2	–	38%
Reference	2	This study	3, 4	5	4, 6	7	2	8	2	1

In addition to the mutations listed in this table, several missense variants and in-frame indels with unknown functions have been found in patients with isolated cardiovascular anomalies and in those with DGS/VCFS-like phenotype [4].
NLS: nuclear localization signal; TAD: transactivation domain; LOF: loss-of-function; N.D.: not described; N.E.: not examined; GOF: gain-of-function; Del: deletion; and Dup: duplication.
[a]According to NM_080647.
[b]Suggestive of 22q11.2 deletion syndrome.
[c]Velopharygeal insufficiency.
[d]Hypocalcemia is included.
[e]Two of the three subjects have been examined for hypoplastic thymus.
[f]One of the five subjects has been examined for hypoplastic thymus.
[g]These two mutations have been inherited from apparently normal mothers.
[h]The c.1293-1315del23 has been described as c.1320-1342del23 in the original report [5].
[i]Although the natural NLS has been disrupted, a new NLS-compatible motif (RGRRRRCR) has been created on the added amino acid sequence.
[j]Another deceased individual in this family also has similar clinical features.
[k]These two mutations have been identified in *TBX1* analyses for patients with cardiovascular anomalies only.
[l]The mutant protein is aggregated in the cytoplasm and the nucleus.
[m]Gain-of-function effects have been found by *in vitro* studies [8].
doi:10.1371/journal.pone.0091598.t002

phenotype. Application of such powerful methods will serve to identify a causative gene in genetically heterogeneous disorders.

Supporting Information

Figure S1 Comparison of amino acid sequence of human *TBX1C* and mouse *Tbx1*. The T-box is highlighted in yellow, and the nuclear localization signal in light blue. The region for transactivation domain is surrounded by squares. The Y highlighted in red denotes the amino acid residue where the frameshift mutation in this family has taken place.
(TIF)

Figure S2 Analysis of c.2968A>G SNP (p.R990G, rs1042636) with a gain-of-function effect in exon 7 of *CASR*. The SNP pattern is not co-segregated with the presence or absence of hypocalcemia.
(TIF)

Table S1 Summary of heterozygous non-synonymous variants.
(PDF)

Table S2 A list of variants that are present in groups 1+2 and absent from group 3.
(PDF)

Table S3 A list of variants that are present in group 1 and absent from groups 2+3.
(PDF)

Table S4 A list of variants that are present in group 1 and absent from group 2.
(PDF)

Table S5 A list of variants that are present in group 2 and absent from group 1.
(PDF)

References

1. Ryan AK, Goodship JA, Wilson DI, Philip N, Levy A, et al. (1997) Spectrum of clinical features associated with interstitial chromosome 22q11 deletions: a European collaborative study. J Med Genet 34: 798–804.
2. Yagi H, Furutani Y, Hamada H, Sasaki T, Asakawa S, et al. (2003) Role of TBX1 in human del22q11.2 syndrome. Lancet 362: 1366–1373.
3. Baldini A (2005) Dissecting contiguous gene defects: TBX1. Curr Opin Genet Dev 15: 279–84.
4. Gong W, Gottlieb S, Collins J, Blescia A, Dietz H, et al. (2001) Mutation analysis of TBX1 in non-deleted patients with features of DGS/VCFS or isolated cardiovascular defects. J Med Genet 38: E45.
5. Paylor R, Glaser B, Mupo A, Ataliotis P, Spencer C, et al. (2006) Tbx1 haploinsufficiency is linked to behavioral disorders in mice and humans: implications for 22q11 deletion syndrome. Proc Natl Acad Sci U S A 103: 7729–7734.
6. Rauch R, Hofbeck M, Zweier C, Koch A, Zink S, et al. (2010) Comprehensive genotype-phenotype analysis in 230 patients with tetralogy of Fallot. J Med Genet 47: 321–331.
7. Griffin HR, Töpf A, Glen E, Zweier C, Stuart AG, et al. (2010) Systematic survey of variants in TBX1 in non-syndromic tetralogy of Fallot identifies a novel 57 base pair deletion that reduces transcriptional activity but finds no evidence for association with common variants. Heart 96: 1651–1655.
8. Zweier C, Sticht H, Aydin-Yaylagül I, Campbell CE, Rauch A (2007) Human TBX1 missense mutations cause gain of function resulting in the same phenotype as 22q11.2 deletions. Am J Hum Genet 80: 510–517.
9. Daw SCM, Taylor C, Kraman M, Call K, Mao J, et al. (1996) A common region of 10p deleted in DiGeorge and velocardiofacial syndromes. Nat Genet 13: 458–461.
10. McDonnell SK, Riska SM, Klee EW, Thorland EC, Kay NE, et al. (2013) Experimental designs for array comparative genomic hybridization technology. Cytogenet Genome Res 139: 250–257.
11. Wang Z, Liu X, Yang B-Z, Gelernter J (2013) The role and challenges of exome sequencing in studies of human diseases Front Genet doi: 10.3389/fgene.2013.00160.
12. Li H, Durbin R (2009) Fast and accurate short read alignment with Burrows-Wheeler transform. Bioinformatics 25: 1754–1760.
13. McKenna A, Hanna M, Banks E, Sivachenko A, Cibulskis K, et al. (2010) The Genome Analysis Toolkit: a MapReduce framework for analyzing next-generation DNA sequencing data. Genome Res 20: 1297–1303.
14. Wang K, Li M, Hakonarson H (2010) ANNOVAR: functional annotation of genetic variants from high-throughput sequencing data. Nucleic Acids Res 38: e164.
15. Williams SR, Aldred MA, Der Kaloustian VM, Halal F, Gowans G, et al (2010). Haploinsufficiency of HDAC4 causes brachydactyly mental retardation syndrome, with brachydactyly type E, developmental delays, and behavioral problems. Am J Hum Genet 87: 219–228.
16. Kong S, Amos CI, Luthra R, Lynch PM, Levin B, et al. (2000) Effects of cyclin D1 polymorphism on age of onset of hereditary nonpolyposis colorectal cancer. Cancer Res 60: 249–252.
17. Zatyka M, da Silva NF, Clifford SC, Morris MR, Wiesener MS, et al (2002). Identification of cyclin D1 and other novel targets for the von Hippel-Lindau tumor suppressor gene by expression array analysis and investigation of cyclin D1 genotype as a modifier in von Hippel-Lindau disease. Cancer Res 62: 3803–3811.
18. Holbrook JA, Neu-Yilik G, Hentze MW, Kulozik AE (2004) Nonsense-mediated decay approaches the clinic. Nat Genet 36: 801–808.
19. Stoller JZ, Epstein JA (2005) Identification of a novel nuclear localization signal in Tbx1 that is deleted in DiGeorge syndrome patients harboring the 1223delC mutation. Hum Mol Genet 14: 885–892.
20. Vezzoli G, Terranegra A, Arcidiacono T, Biasion R, Coviello D, et al. (2007) R990G polymorphism of calcium-sensing receptor does produce a gain-of-function and predispose to primary hypercalciuria. Kidney Int 71: 1155–1162.
21. Ohtani I, Schuknecht HF (1984) Temporal bone pathology in DiGeorge's syndrome. Ann Otol Rhinol Laryngol 93(3 Pt 1): 220–224.
22. Kawame H, Adachi M, Tachibana K, Kurosawa K, Ito F, et al. (2001) Graves' disease in patients with 22q11.2 deletion. J Pediatr 139: 892–895.

Author Contributions

Conceived and designed the experiments: TO YM. Performed the experiments: T. Niihori SN FK MF YA. Analyzed the data: T. Nagashima RF KN. Contributed reagents/materials/analysis tools: KN. Wrote the manuscript: TO. Collected the clinical findings: NT MK.

JIMD Reports
DOI 10.1007/8904_2014_320

RESEARCH REPORT

Seven Novel Mutations in Bulgarian Patients with Acute Hepatic Porphyrias (AHP)

Sonya Dragneva · Monika Szyszka-Niagolov · Aneta Ivanova · Lyudmila Mateva · Rumiko Izumi · Yoko Aoki · Yoichi Matsubara

Received: 23 February 2014 / Revised: 07 May 2014 / Accepted: 09 May 2014 / Published online: 6 July 2014

Abstract Acute intermittent porphyria (AIP), variegate porphyria (VP), and hereditary coproporphyria (HCP) are caused by mutations in the hydroxymethylbilane synthase (HMBS), protoporphyrinogen oxidase (PPOX), and coproporphyrinogen oxidase (CPOX) genes, respectively. This study aimed to identify mutations in seven Bulgarian families with AIP, six with VP, and one with HCP. A total of 33 subjects, both symptomatic ($n = 21$) and asymptomatic ($n = 12$), were included in this study. The identification of mutations was performed by direct sequencing of all the coding exons of the corresponding enzymes in the probands. The available relatives were screened for the possible mutations. A total of six different mutations in HMBS were detected in all seven families with AIP, three of which were previously described: c.76C>T [p.R26C] in exon 3, c.287C>T [p.S96F] in exon 7, and c.445C>T [p.R149X] in exon 9. The following three novel HMBS mutations were found: c.345-2A>C in intron 7–8, c.279-280insAT in exon 7, and c.887delC in exon 15. A total of three different novel mutations were identified in the PPOX gene in the VP families: c.441-442delCA in exon 5, c.917T>C [p.L306P] in exon 9, and c.1252T>C [p.C418R] in exon 12. A novel nonsense mutation, c.364G>T [p.E122X], in exon 1 of the CPOX gene was identified in the HCP family. This study, which identified mutations in Bulgarian families with AHP for the first time, established seven novel mutation sites. Seven latent carriers were also diagnosed and, therefore, were able to receive crucial counseling to prevent attacks.

Abbreviations

AHP	Acute hepatic porphyrias
AIP	Acute intermittent porphyria
ALA	δ-Aminolevulinic acid
CPOX	Coproporphyrinogen oxidase
HCP	Hereditary coproporphyria
HMBS	Hydroxymethylbilane synthase
PBG	Porphobilinogen
PPOX	Protoporphyrinogen oxidase
VP	Variegate porphyria

Introduction

Acute intermittent porphyria (AIP) (OMIM 176000), variegate porphyria (VP) (OMIM 176200), and hereditary coproporphyria (HCP) (OMIM 121300) are autosomal dominant, low-penetrant inborn errors of the heme biosynthesis pathway that result in the decreased activity of hydroxymethylbilane synthase (HMBS) (EC 4.3.1.8), protoporphyrinogen oxidase (PPOX) (EC 1.3.3.4), and coproporphyrinogen oxidase (CPOX) (EC 1.3.3.3), respectively.

AIP, VP, and HCP present with clinically identical recurrent neurovisceral attacks. Additionally, erosive bullous cutaneous lesions and hyperpigmentation on sun-exposed areas are more common in VP than in HCP (Sassa 2006). The acute attacks include three major classes of symptoms: gastrointestinal, neurological, and psychiatric. These symptoms are represented by severe abdominal pains, motor neuropathy, depression, and psychosis. The most common factor trigger-

Communicated by: Eva Morava, MD PhD

Competing interests: None declared

S. Dragneva (✉) · M. Szyszka-Niagolov · A. Ivanova · L. Mateva
Clinic of Gastroenterology and Hepatology, University Hospital "Saint Ivan Rislki", Sofia, Bulgaria
e-mail: sonya.dragneva@gmail.com

R. Izumi · Y. Aoki · Y. Matsubara
Department of Medical Genetics, School of Medicine, Tohoku University, Sendai, Japan

ing these attacks is the use of numerous porphyrinogenic drugs. Infections, alcohol, a low-calorie diet, and natural sex hormones fluctuations in women, related to menstrual cycle and pregnancy can also provoke attacks (Kappas et al. 1995).

The diagnosis of acute porphyric attack is based on both clinical manifestations and typical biochemical abnormalities. The main laboratory finding is the dramatic increase of the porphyrin precursors porphobilinogen (PBG) and δ-aminolevulinic acid (ALA) in urine. The exact distinction between the three different diseases requires measuring the urinary and fecal porphyrin excretion patterns, which are characteristic for each enzymatic defect. A fluorescence scan of native plasma is also an important diagnostic criterion, presenting (or not) a characteristic peak for each entity (Sassa 2006; Hift et al. 2004). Decreased levels of HMBS activity in AIP, PPOX activity in PV, and CPOX activity in HCP clarify the diagnosis in the proband and establish the enzymatic defect in the latent carriers (Meyer et al. 1972; Deybach et al. 1981). Unfortunately, when measuring enzymatic activities, results similar to the reference values may bring in uncertainty in the precise diagnosis of the latent carriers (Mustajoki 1981). Thus, the optimal strategy for the detection of these individuals includes the implementation of molecular genetic methods (Whatley et al. 2009).

At least 600 different mutations in the HMBS, PPOX, and CPOX genes have been identified so far (www.hgmd.cf.ac.uk). Most of these mutations are specific to one or a few families, although a founder effect has been clearly demonstrated for both AIP and VP (Thunnel et al. 2006; Meissner et al. 1996). Most AIP, VP, and HCP carriers are heterozygotes. Mutations are heterogeneous and are comprised of single nucleotide substitutions, small insertions and deletions. Recently, large insertions/deletions have been described in the HMBS, PPOX, and CPOX genes (Whatley et al. 2009; Barbaro et al. 2013). In Bulgaria, during a 50-year period as the sole porphyria service at University Hospital "Saint Ivan Rislki" Sofia, 35 families with AIP, 20 with VP, and 2 with HCP have been diagnosed, treated, and followed up. However, the molecular analysis of the patients with AIP, VP, and HCP has not yet been performed. The aim of this study was to identify mutations in the HMBS, PPOX, and CPOX genes in Bulgarian families with acute hepatic porphyrias.

Materials and Methods

Patients

Seven independent index cases with AIP were included. The diagnosis was based on clinical symptoms and increased urinary PBG and ALA values. Decreased levels of HMBS activity in erythrocytes and the absence of a plasma fluorescence peak at 624–627 nm confirmed the diagnosis of AIP. Six independent index cases with VP were also studied. The diagnosis of these patients included the evaluation of the clinical symptoms, a typical plasma fluorescence peak at 624–627 nm, elevated urinary PBG and ALA levels during acute attacks and increased stool porphyrins, with a predominance of protoporphyrin over coproporphyrin in the cases with cutaneous symptoms. One patient with HCP was included. The diagnosis was based on the symptoms that occurred during acute attack, increased urinary PBG and ALA levels, markedly increased total porphyrins in the urine, and a plasma fluorescence peak at 618 nm. Molecular analysis of the HMBS, PPOX, and CPOX genes confirmed the precise diagnosis. These 14 probands were diagnosed, treated, and followed up in the Porphyria Unit of "Saint Ivan Rilski" University Hospital Sofia. The precise places of birth and the pedigree trees of the patients were determined, with no apparent signs of consanguinity. Once the diagnosis of AIP was confirmed, the HMBS activity was evaluated in the available asymptomatic family members. A total of 33 individuals, including the probands and asymptomatic relatives, from 15 families with AIP, VP, and HCP gave their written consent to participate in this study, which was approved by the Ethics Committee.

Methods

Biochemical Measurements

PBG and ALA levels in the urine were measured according to the method described by Mauzarell and Granick (1956). Urinary and fecal porphyrins were assessed according to the method of Rimington (1971). Total fecal total porphyrin levels were measured according to the method of Lockwood et al. (1985). Total porphyrin levels in urine were evaluated according to our modification and optimization of the method described by Deacon and Elder (2001). HMBS activity in the erythrocytes was determined according to the method described by Adjarov et al. (1994). Plasma fluorescence scanning was performed on a Perkin–Elmer fluorescence spectrophotometer MPF 43, with an excitation wavelength of 398 nm and an emission spectrum from 580 to 700 nm.

Identification of Mutations

Genomic DNA was isolated from peripheral whole blood samples using the innuPREP Blood DNA Midi kit (Analytik Jena Life Science, Germany) according to the manufacturer's protocol. PCR amplification of exons 1 to

Table 1 Clinical and biochemical data and mutations detected in the HMBS gene in families with acute intermittent porphyria

Fam	Pts	Sex	Age/age at first symptoms	Nucleotide change	Amino acid change	Symptoms	HMBS	No. of acute attacks	Urine		TF	TT
									PBG	ALA		
I	P1	F	40/19	c.76C>T	p.R26C	+	18.7	1	715	95	MC	Glu
	Fa	M	65/44	c.76C>T	p.R26C	+	20.1	–	129	122	Inf + M	–
II	P2	F	47/20	c.279-280insAT[a]	Frameshift	+	14.1	2	153	42.7	–	C + Glu
	Sc1	F	45/26	c.279-280insAT[a]	Frameshift	+	10	2	189	–	P	Glu
	Sc2	F	37/30	c.279-280insAT[a]	Frameshift	+	14.3	1	304	–	Inf + M	Glu
	Mo	F	69	c.279-280insAT[a]	Frameshift	–	14	–	–	–	–	–
III	P3	F	44/24	c.887delC[a]	Frameshift	+	20.6	1	320	19.4	MC	Hem
	So	M	20	Neg		–	34.3	–	–	–	–	–
IV	P4	F	27/22	c.445C>T	p.R149X	+	ND	2	955	100	MC	Glu
	Mo	F	50	c.445C>T	p.R149X	+	ND	–	350	78	MC	–
	Si	F	28	Neg	–	–	ND	–	–	–	–	–
V	P5	F	59/39	c.345-2A>C[a]	Splice acceptor site	+	18.7	1	341	214	Inf + M	C + Glu
VI	P6	F	43/25	c.287C>T	p.S96F	+	25.1	1	421	45	MC	Glu
	D	F	21	c.287C>T	p.S96F	–	ND	–	–	–	–	–
VII	P7	F	42/28	c.287C>T	p.S96F	+	ND	1	384	130	MC	Glu
	D	F	15	c.287C>T	p.S96F	–	ND	–	18.2	–	–	–

Fam family, *Pts* patients, *P* proband number, *Fa* father, *Sc* second cousin, *Mo* mother, *So* son, *Si* sister, *D* daughter, *F* female, *M* male, *HMBS* hydroxymethylbilane synthase activity in the erythrocytes, normal range: 25–45 pkat/gHb, *PBG* porphobilinogen, normal value: <15 μmol/24 h, *ALA* δ-aminolevulinic acid, normal range: 11.4–57.2 μmol/24 h, *TF* triggering factor, *Inf* infection, *M* medication, *MC* menstrual cycle, *P* pregnancy, *TT* treatment, Glu, 10% glucose i.v. infusion, *C* cimetidine, *Hem* Hem-arginate (Normosang), *ND* not determined

[a] Novel mutations identified

15 for HMBS, exons 1 to 13 for PPOX, and exons 1 to 7 for CPOX, with corresponding flanking intron–exon boundaries, was performed; the primers and PCR conditions are available upon request. The PCR products were automatically sequenced using the BigDye Terminator v3.1 Cycle Sequencing Kit and a 3500xL Genetic Analyzer (Applied Biosystems, Foster City, USA).

To prove the rarity of the identified novel missense mutations, the corresponding exons of the HMBS and PPOX genes were screened in 96 control DNA samples. In silico prediction of the pathogenicity of these mutations was determined by the HumVar score using the PolyPhen-2 tool (http://genetics.bwh.harvard.edu/pph2/).

Results and Discussion

Detailed clinical, biochemical, and genetic data are presented in Table 1 for the AIP families and in Table 2 for the VP and HCP families. In three of our female AIP patients, the attacks were related to the patient's menstrual cycle. Infections and/or medications played a triggering role in three AIP and four VP cases, as well as in the HCP patient. Nine subjects with AIP manifested with one or two acute attacks. Some patients (family I-F, family II-P2 and II-Sc1, family IV-P4 and family V-P5) suffered chronic symptoms, including fatigue, lower back pain, paresthesia in the lower limbs, and depression. The proband P2 had suffered from two unrecognized acute attacks and had residual paresis at the time of presentation in our clinic. She also had chronic neurological symptoms when Cimetidine treatment was applied. During the 6 months course of Cimetidine administration, a reduction in porphyrin precursors levels and clinical improvement was achieved. Family V-P5 suffered from one acute attack following infection and antibiotic treatment after surgery. She also had chronic neurological symptoms. Cimetidine was administered after the acute onset, but over the first weeks the pains worsened and no biochemical improvement was noticed. Both acute and cutaneous symptoms were present in four symptomatic VP patients, and only acute symptoms were present in one patient and only cutaneous symptoms in four patients. All VP patients manifested with a single acute attack, and only family III-So exhibited chronic symptoms similar to those observed in AIP. The majority of our VP patients presented with severe photodermatosis alone or accompanying acute

Table 2 Clinical, biochemical and genetic characteristics of families with variegate porphyria and hereditary coproporphyria

Fam	Pts	Sex	Age/age at first symptom	Gene	Nucleotide change	Amino acid change	Symptoms		Plasma scan	Urine					Feces					
							Acute	Skin		PBG	ALA	TPu	Uro	Cop	TPf	Uro	Cop	Proto	TF	TT
I-VP	P1	F	28/21	PPOX	c.441-442delCA	Frame-shift	+	–	626	37	40	4,675	2,340	2,335	–	–	–	–	Inf + M	Glu
	D	F	11	PPOX	c.441-442delCA	Frame-shift	–	–	ND	–	–		–	–	–	–	–	–	–	–
II-VP	P2	F	30/24	PPOX	c.917T>C	p.L306P	+	+	626	383		7,076	–	–	2,422[a]	–	–	–	Inf + M	Glu
	So	M	3	PPOX	c.917T>C	p.L306P	–	–	Neg	2	13	0	–	–	0.6	–	–	–	–	–
III-VP	P3	M	69/39	PPOX	c.917T>C	p.L306P	–	+	626	3	19	1,326	143	1,183	671	84	241	346		Ph
	So	M	43/30	PPOX	c.917T>C	p.L306P	+	+	627	75	223	930	–	–	1,753	–	–	–	–	Glu
	G	M	10	PPOX	Neg	–	–	–	Neg	3	15	120	–	–	138	–	–	–	–	–
IV-VP	P4	F	80/45	PPOX	c.917T>C	p.L306P	–	+	626	2.2	16.8	1,340	79	1,261	3,182	890	662	1,630	–	Ph
	D	F	58	PPOX	c.917T>C	p.L306P	–	+	626	3.7	30	199[a]	–	–	1,202[a]	–	–	–	–	–
	So	M	48	PPOX	c.917T>C	p.L306P	–	–	Neg	5	32	0	–	–	142	–	–	–	–	–
V-VP	P5	F	31/25	PPOX	c.1252T>C	p.C418R	+	+	626	505	309	14,326	–	–	–	–	–	–	Inf + M	
	Si	F	38/25	PPOX	c.1252T>C	p.C418R	+	+	626	11[a]	33[a]	217[a]	–	–	–	–	–	–	Inf	
	So	M	19	PPOX	Neg	–	–	–	Neg	7	29	68	–	–	–	–	–	–	–	
	Ni	F	16	PPOX	c.1252T>C	p.C418R	–	–	ND	–	–		–	–	–	–	–	–	–	
	Nf	M	17	PPOX	Neg	–	–	–	ND	–	–		–	–	–	–	–	–	–	
VI-VP	P6	M	63/35	PPOX	c.1252T>C	p.C418R	–	+	626	8	66	626	74	552	268	3	88	177	–	
I-HCP	P	F	22/22	CPOX	c.364G>T	p.E122X	+	–	618	53	63	5,100	1,425	4,100	4,960	–	–	–	Inf + M	Glu

Fam, family, *Pts* patients, *P* proband number, *Si* sister, *D* daughter, *Ni* niece, *Nf* nephew, *G* grandson, *F* female, *M* male, *PBG* porphobilinogen, normal value: <15 μmol/24 h, *ALA* δ-aminolevulinic acid, normal range: 11.4–57.2 μmol/24 h, *TPu* total porphyrins in urine, normal values <200 nmol/24 h, *Plasma scan* plasma fluorescence emission peak in nm, *TPf* total porphyrins in feces, normal values <150 nmol/g dry weight, *Uro* uroporphyrin, normal values: <36 nmol/24 h in urine, <1 nmol/g dry weight in feces, *Cop* coproporphyrins, normal values: <122 nmol/24 h in urine, <26 nmol/g dry weight in feces, *Proto*, protoporphyrins, normal value: <80 nmol/g dry weight in feces, *TF* triggering factor, *Inf* infection, *M* medication, *TT* treatment, *Glu* 10% glucose i.v. infusion, *Ph* photoprotection, *ND* not determined, *Neg* no emission peak on plasma scan

[a] Mark, values measured after resolution of the acute attack